UNIVERSITY
OF OSLO

Master thesis – Fall 2023

Perturbations of perineuronal nets in the medial prefrontal cortex during learning of a visual discrimination task

Overexpression of chondroitin 6-sulfotransferase-1 and CRISPR activation of ADAMTS15.

Sandra Kristine Stølen Bryne

Master of Biosciences
60 credits
Department of Biosciences
Faculty of Mathematics and Natural Sciences

2023

Perturbations of perineuronal nets in the medial prefrontal cortex during learning of a visual discrimination task – Overexpression of chondroitin 6-sulfotransferase 1 and CRISPR activation of ADAMTS15

Sandra K. S. Bryne

http://www.duo.uio.no/

Print: Grafisk senter, University of Oslo

Acknowledgements

The work presented in this thesis was performed in the CINPLA research group, Department of Biosciences, University of Oslo, under the supervision of my five supervisors, doctoral research fellow Guro Hélen Vatne, Sverre Grødem, Elise Reppe Olsen, Dr. Elise Holter Thompson, and Professor Marianne Fyhn.

Firstly, I would like to thank my supervisors, Guro Hélen Vatne and Sverre Grødem, for helping me along the way, guiding me in molecular work and theory and teaching me impressive bouldering skills. I want to thank my supervisor, Dr. Elise Holter Thompson, for guidance in the animal experiments and the lab. Thank you to my supervisor, Marianne Fyhn, for letting me be a part of CINPLA and for your valuable feedback. Thank you to my supervisor, Elise Reppe Olsen, for stepping in on short notice, teaching me how to become a brain surgeon, for the extensive help with the writing, and for the general care.

I would also like to thank everyone in CINPLA for making these years valuable, for great conversations and for all the help. Thank you to all my fellow master students in 2619 for all the great conversations and for always supporting. I also want to thank Viktor and Ali, the OG 2615, for becoming my closest friends. And again, thank you, Ali, for being my partner in crime during this master's. A special thanks goes to my family for all the support and care, and thank you Ivan, for always being by my side.

Abstract

The perineuronal nets (PNNs) are condensed extracellular matrix structures surrounding the cell soma and proximal dendrites of neurons. The PNNs are thought to contribute to the reduced plasticity of the adult brain. This is supported by the reduced plasticity at the time of their emergence and by solid evidence that removing the PNNs unlocks plasticity in the adult. However, the mechanisms behind the PNN's role in plasticity still remain elusive, and difficulties in precisely targeting the PNNs have rendered this more challenging. Recent studies have revealed a potential role of sulphation patterns and peptidase activity in maintaining heightened plasticity in early development. In the current study, we pilot a new method of PNN perturbations by exploiting the neuron's own mechanisms for regulating the PNNs through adeno associated virus (AAV) delivery. We overexpress the chondroitin-6 sulfotransferase 1 (C6ST1) to increase levels of the carbon-6 sulphation (C6S) seen early in development, and CRISPR activate the proteinase “a disintegrin and metalloproteinase with thrombospondin motifs 15” (ADAMTS15). PNN perturbations were targeted through AAV delivery by microinjections in the medial prefrontal cortex (mPFC) of mice before a visual discrimination task, to assess its effects on learning. The experiments revealed reduced staining of the PNNs in the mPFC, indicating that the new method successfully caused PNN perturbations. Results from the visual discrimination task suggest that the PNN perturbations did not affect the initial learning of the visual discrimination task but significantly affected learning once the visual cues were reversed. This effect cannot be confined to the PNN's role in the mPFC as the virus spread was extensive.

Abbreviations

ECM	Extracellular matrix
CNS	Central nervous system
CSPG	Chondroitin sulfate proteoglycans
PNN	Perineuronal nets
CS-GAG	Chondroitin sulfate glycosaminoglycans
ChABC	Chondroitinase ABC
GABA	Gamma-aminobutyric acid
PV	Parvalbumin
C6S	Carbon-6 sulphation
C6ST1	Chondroitin 6-sulfotransferase 1
C4S	Carbon-4 sulphation
ADAMTS	A disintegrin and metalloproteinase with thrombospondin motifs
PFC	Prefrontal cortex
mPFC	Medial prefrontal cortex
PL	Prelimbic cortex
IL	Infralimbic cortex
AAV	Adeno associated virus
DNA	Deoxyribonucleic acid
CRISPR	Clustered regularly interspaced short palindromic repeats
RNA	Ribonucleic acids
DSB	Double strand breaks
CRISPRi	CRISPR inhibition
CRISPRa	CRISPR activation
SC	Subcutaneously
NL	Nano litres
PBS	Phosphate-buffered saline
PFA	Paraformaldehyde
ACAN	Aggrecan
qPCR	Quantitative polymerase chain reaction

Table of Contents

1. Introduction

Most people think of memories, either as an image or an animation, which can be triggered by specific stimuli such as the smell of your mother's cooking. However, on the anatomical level, memories are something far different. Behind every thought is a neuronal circuit in the brain responsible for helping us encode and retrieve important information. These circuits have been formed during development, are refined throughout life and are thought to form the basis of our memory. To encode new experiences as memories, changes in the neuronal contacts need to occur. These neuronal contact points are called synapses, and activity can change their strength and efficiency. This ability is termed synaptic plasticity and is believed to be altered by our experiences. Donald O. Hebb (1949) proposed that repeated activity-dependent firing of a neuron will enhance its connection to the post-synaptic neuron, summarised in his saying: "Neurons that fire together wire together." Certain synapses are strengthened and other weakened, all dependent on our activity. This experience-driven synaptic plasticity is essential for the development of neural circuit function, learning, and memory (Bliss & Collingridge, 1993; Romberg et al., 2013).

1.1 Extracellular matrix (ECM)

The synaptic plasticity, crucial to learning and memory, may involve cells or structures around the synapse. One such player is the extracellular matrix (ECM) surrounding cells of different tissues and organs. The ECM serves as the infrastructure around the cells and consists of proteins and carbohydrates, among other molecules. The ECM in the central nervous system (CNS) is different from that of the rest of the body and consists mainly of hyaluronic acid and proteoglycans, including chondroitin sulfate proteoglycans (CSPG), tenascin-R and link proteins (Kwok et al., 2011). The proteoglycans are proteins with polysaccharide chains covalently attached and abundant in the ECM. Many of the significant ECM constituents are synthesised by neurons and glial cells. Both the structure and composition of the ECM affect its biomechanical properties and overall structure (Song & Dityatev, 2018; Theocharis et al., 2016). Beyond its infrastructural

properties, the ECM plays essential roles in development and adulthood. During brain development, it plays a regulatory function. It is necessary to form synapses, guiding axon growth and cell migration, while in adulthood, it likely plays a role in synaptic stability and limiting neuronal reorganisation (Burnside & Bradbury, 2014; Lam et al., 2019). The proteoglycans of the ECM are thought to have an essential role in limiting brain plasticity by stabilising the synapse (Mencio et al., 2021; Miyata et al., 2012).

1.2 Perineuronal net (PNN)

1.2.1 Perineuronal net structure

A condensed ECM structure, discovered in the late 19th century and whose role in brain plasticity has become more evident, is the perineuronal net (PNN) (Golgi, 1898). Anchored to the neuronal cell surface, the PNNs tightly enwrap the cell soma and proximal dendrites of neurons in a lattice-like fashion. The PNNs are aggregated ECM component structures and share many constituents with cartilage (Deepa et al., 2006). A proposed structure of the PNNs is illustrated in Figure 1. In vitro studies have given us valuable information on how the PNNs are composed and linked together (Kwok et al., 2010). Extending from the transmembrane hyaluronan synthases are simple glycosaminoglycans called hyaluronan, making up the backbone of the PNNs. The hyaluronan extends outside the cell surface, forming connections with other components of the PNNs. Connected to the backbone are chondroitin sulphate proteoglycans called lecticans. The lectican family, including aggrecan, neurocan, versican and brevican, are abundant constituents of the PNNs, with aggrecan as the most reoccurring (Jakovljević et al., 2021). CS glycosaminoglycans (CS-GAG) chains are attached in varying amounts in the lecticans protein core. The ECM glycoprotein tenascin R (Tn-R) binds to the lecticans, forming the unique structure of the PNNs. Link proteins bind to both hyaluronan and the CSPGs and stabilises this interaction while keeping the net structure secured to the cell (Kwok et al., 2011). The most commonly used PNN marker is the plant lectin *Wisteria floribunda agglutinin* (WFA), which is thought to bind to one of the repeated disaccharide units of the CS-GAG chains in the lectins (Härtig et al., 2022).

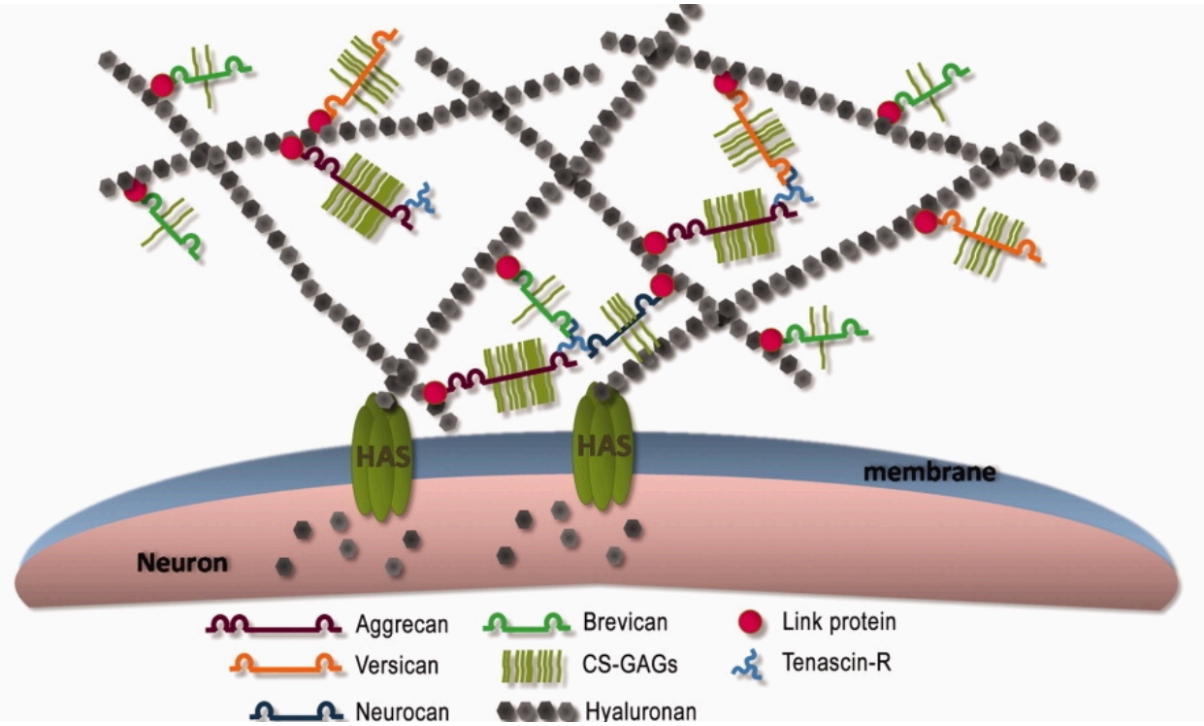

Figure 1: **The proposed structure of the perineuronal nets.** Hyaluronan synthases (HAS) anchor the hyaluronan to the cell surface, while tenascin-R binds to the lecticans and link proteins to stabilize the connections. Adapted from (Kwok et al., 2011).

1.2.2 Perineuronal nets and plasticity

The PNNs are proposed to play an important role in regulating plasticity. Early in development, immature cortical circuits need refinement to elicit adaptable responses to the environment (Berardi et al., 2000). These periods are associated with heightened plasticity and are dependent on activity. The most established model is the ocular dominance shift, where one eye deprived of vision early in life can cause visual impairment continuing into adulthood (Levelt & Hübener, 2012). The same effect is not observed in adult animals, indicating that the stimulus timing is important. Such periods of heightened plasticity early in life are called critical periods and are restricted time windows where the cortical circuits of the brain are dependent on adequate stimuli for their formation (Levelt & Hübener, 2012). The closure of these periods is related to the level of inhibitory activity and is, therefore, dependent on the inhibitory system. Interestingly, the formation of the PNNs seems to coincide with the closure of these periods and are thought to contribute to the restricted plasticity seen in adults as they may stabilise the formed connections (Carulli et al., 2010; Pizzorusso et al., 2002). As the PNNs aggregate tightly around the neurons,

they are thought to control the level of synapse formation on to the neurons by only opening up for synaptic contact in the “holes” of the lattice (Matthews et al., 2002) (Figure 2A). This restriction of plasticity may be needed to retain acquired information and skills throughout life, but the large re-organisation of neural circuits seen in juvenile animals is probably unnecessary in adulthood when established circuits have already been made. However, the mechanisms by which the PNNs modulate or restrict plasticity are not fully understood. To study the PNN's role in plasticity, a bacterial enzyme, chondroitinase ABC (ChABC), has been widely used. This enzyme has been found to digests the lecticans CS-GAG chains of the PNNs, causing short windows of increased plasticity in the adult brain (Kwok et al., 2008) (Figure 2B). PNN removal in the visual cortex using ChABC was seen to reduce the inhibitory activity, resembling the increased plasticity seen in young animals (Lensjø et al., 2017). However, this enzyme is not specific to the CSPGs in the PNNs but also digests CPSGs in the surrounding ECM and as only 2-5% of the CSPGs aggregate in PNNs, its digestion can cause confounding effects (Deepa et al., 2006). Digestions with the ChABC have, however, been shown to increase the plasticity in several brain areas and enhance axon regeneration in CNS injuries by removing the inhibitory CSPGs around the injury site (Lensjø, Lepperød, et al., 2017; Moon et al., 2001; Pizzorusso et al., 2002). The PNNs have been implicated in many functions like memory (Favuzzi et al., 2017; Thompson et al., 2018; Tsien, 2013), behaviour and cognition (Happel et al., 2014; Hylin et al., 2013), scaffolding for ECM molecules (Fawcett et al., 2019), and protection neurons from certain pathologies (Brückner et al., 1999). Although the PNNs have been implicated in many processes, their exact function remains elusive. What furthers this problem is the methods used for PNN research. These are usually not specific, making the PNNs' contribution difficult to detangle. New methods are needed to unravel the specific functions of the PNNs and how these are regulated.

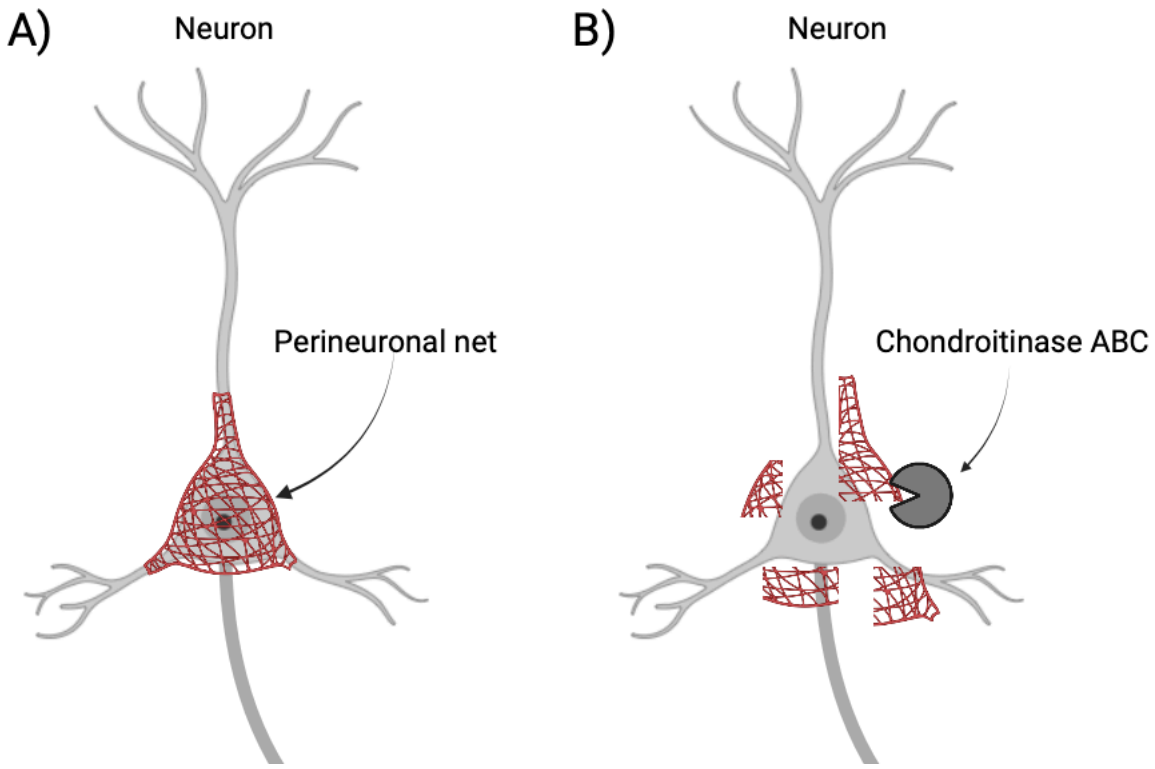

Figure 2: Perineuronal nets and digestion by the enzyme chondroitinase ABC.

A) Perineuronal nets surrounding neuron in a lattice-like structure**. B)** Digestion of the PNNs by cleavage of the CSPGs. Created with BioRender.

1.2.3 Parvalbumin inhibitory neurons

18/09/2023 04:28:00Most inhibitory interneurons release the inhibitory neurotransmitter gamma-aminobutyric acid (GABA), which is the most abundant neurotransmitter in the brain. The GABAergic interneurons are important for maintaining the excitation and inhibitory balance in the brain, and their maturation is considered important for the onset of critical periods (Levelt & Hübener, 2012). The PNNs predominantly surround GABAergic inhibitory neurons expressing the calcium binding protein parvalbumin (PV) in the neocortex, but PNNs have been observed surrounding excitatory pyramidal neurons in other brain areas (Lensjø, Christensen, et al., 2017; Lupori et al., 2023; Miao et al., 2014). The PV interneurons have fast-firing properties which allow them to fire action potentials in high frequencies important for the regulation of neuronal network activity, as these neurons synapse onto excitatory pyramidal cells and can regulate their output (Erisir et al., 1999; Juarez & Martínez Cerdeño, 2022; Nahar et al., 2021). As the PNNs form around these neurons around the end of the critical periods, they both seem important for regulating plasticity and stabilising the neuronal networks in the brain.

1.2.4 Sulphation patterns in the CSPGs

As each of the lecticans contains a lot of CS-GAG chains, the sulphation patterns may affect the regulation of the PNNs and their properties. However, how these sulphation patterns affect the PNNs is still an area of investigation. The CS-GAG chains, composed of repeated units of N-acetyl-D-galactosamine and D-glucuronic acid, can be sulphated at different positions, defining the CS structural diversity and binding properties (Deepa et al., 2002; Maeda et al., 2003). The D-glucuronic acid can be sulphated in position 2 and N-acetyl-D-galactosamine in the 4^{th} and 6^{th} positions, composing a range of sulphated CS variants defined by their difference in sulphation position and combination (Figure 3). The sulphation of carbon 6 (C6S) of the N-acetyl-D-galactosamine is catalysed by chondroitin 6-sulfotransferase 1 (C6ST1), while the carbon-4 sulphation (C4S) is catalysed by chondroitin 4-sulfotransferase 1 (Miyata & Kitagawa, 2016). The C6S sulphation is more permissive to plasticity, while the C4S is more inhibitory (Yang et al., 2021). In the developing brains of mice and chickens, a shift in these sulphation patterns has been observed (Kitagawa et al., 1997; Miyata et al., 2012). Higher levels of the C6S are seen early in development and gradually decrease, while the opposite occurs for the C4S (Miyata et al., 2012). This change in sulphation causes a shift in the C4S/C6S ratio, which may be important in regulating the plasticity in development. As the C4S increases after development, it might make the CSPG more inhibitory, which could partly explain the decrease in plasticity in adults. This decrease in C6S also seems to play a role in the closure of the critical periods and in the aggregation of the PNN towards the end of this period (Carulli et al., 2010). A study overexpressing the C6ST1 in transgenic mice saw that the time course of PNN formation was similar to the change in C4S/C6S ratio and that this increase in C6S led to a reduced number of PNN stained by WFA (Miyata et al., 2012). The sulphation patterns might, therefore, be important for the formation of the PNNs. These findings indicate an important role of sulphation patterns in regulating plasticity and development. Therefore, studying the ratio of C6S/C4S is of interest to understanding the changes in plasticity, how it is regulated and how it affects the PNNs.

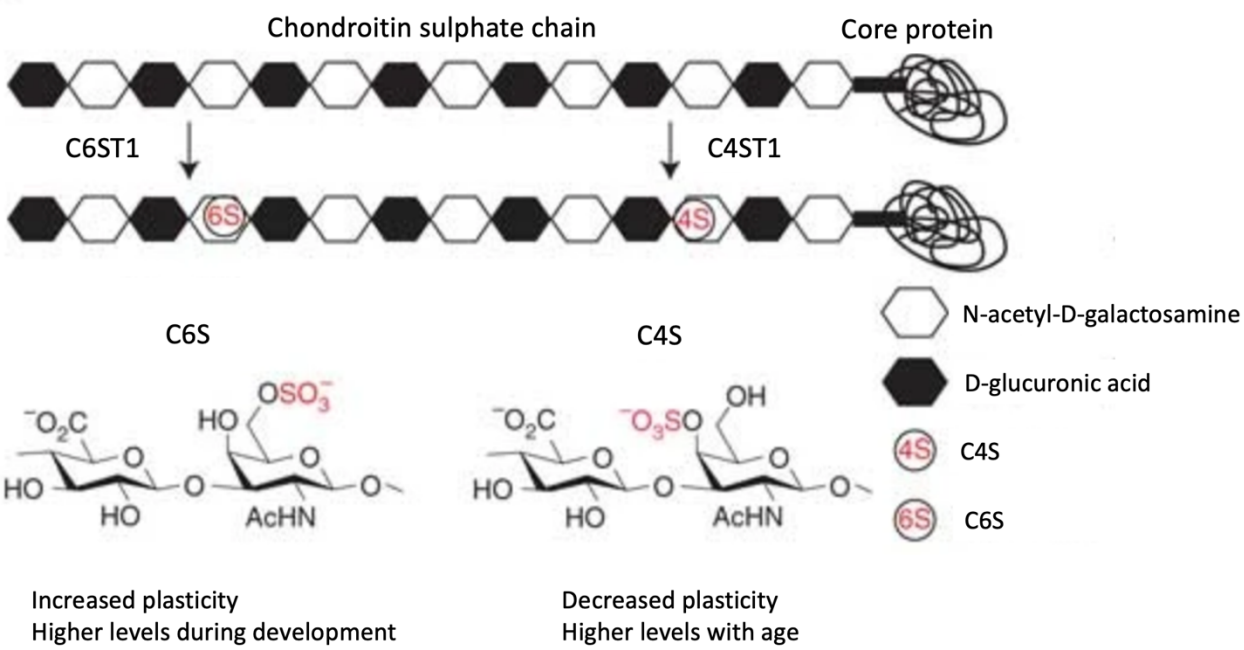

Figure 3: Sulphation pattern in the chondroitin sulphate proteoglycan chains. Sulphation of the 6th (C6S) and 4th carbon (C4S) of the N-acetyl-D-galactosamine changes the properties of the CSPGs. Adapted from (Miyata et al., 2012).

1.2.5 Modulation of the PNNs by metalloproteinases

It is proposed that the PNN structures remain sensitive to sensory input and do not remain static in adult animals, indicating a role of PNN modifications (Wang & Fawcett, 2012). However, the processes behind the modulation of the PNNs are not fully understood. Since the ECM turnover is slow, lasting approximately hours to days, it cannot explain the rapid changes in synaptic plasticity during learning and memory alone (Fawcett et al., 2019; Lin et al., 2007). The activity of metalloproteinases has, therefore, been suggested to be important for PNN remodelling (Fawcett et al., 2019). One of the families of metalloproteinases is the metzincins, which are zinc-dependent proteinases. This family include the matrix metalloproteinases, a disintegrin and metalloproteinase with thrombospondin motifs (ADAMTS), among others. The release of these matrix metalloproteinases by neurons has been related to cellular activity, modulation of the ECM and is thought to be involved in memory and plasticity (Tsilibary et al., 2014). The ADAMTS family consists of many lectican-cleaving proteinases. The ADAMTS15 and ADAMTS4 are aggrecan degrading proteinases found in the hippocampus and neocortex (Brocker et al., 2009; Levy et al.,

2015). A study by Rossier et al., (2015) found that two ADAMTSs, the ADAMTS8 and ADAMTS15, seemed to be preferentially expressed in PV interneurons expressing PNNs. Interestingly, mRNA levels of the same metalloproteinase ADAMTS15 increased in the postnatal days in which developmental processes as synaptogenesis and circuit formation occur in the hippocampus (Levy et al., 2015). Based on these findings, and the ADAMTS15 upregulation under development, it seems likely that the metalloproteinase ADAMTS15 is needed for developmental regulation. As this upregulation is increased before the formation of the PNNs and due to its aggrecan cleaving properties, it might play an important role in the timing and regulation of PNN formation although this remains elusive.

1.3 Medial prefrontal cortex

The prefrontal cortex (PFC) is a part of the frontal lobe and is one of the last brain areas to mature (Johnson et al., 2009). This slow maturation is likely associated with its role in higher-order executive functions as cognition, cognitive flexibility, goal-directed behaviour, reward, motivation, and emotional regulation (Hamel et al., 2022; Jett et al., 2017; Miller & Cohen, 2001; Robbins & Arnsten, 2009). An important region of the PFC is the medial prefrontal cortex (mPFC) and is usually divided into three areas: anterior cingulate cortex, prelimbic cortex (PL) and infralimbic cortex (IL) based on the subregions cytoarchitecture (Anastasiades & Carter, 2021) (Figure 4). The division of the mPFC is, however, still a topic of debate, as high variability is seen across species (Carlén, 2017; Laubach et al., 2018). The mPFC is thought to play a crucial role in orchestrating inputs from cortical and subcortical areas and updating this information (Arain et al., 2013). Studies of the mPFC connections in rodents have supported this theory, showing long and reciprocal connections to other brain areas (Anastasiades & Carter, 2021; Zhang et al., 2016). Connections of the mPFC to the nucleus accumbens have been implicated with adaptive goal-directed responses and drug-seeking behaviour (Hamel et al., 2022; Slaker et al., 2015). A study of cocaine-seeking behaviour in rats found that removing the PNNs in the mPFC impaired the initial learning and retrieval of cocaine-induce conditioned place preference memory, which indicating a change in the plasticity of the memory (Slaker et al., 2015). A study inactivation of the mPFC subregions: PL and IL, found that it impaired reinforced and nonreinforced responding when discriminating between rewarding and punishment cues (Hamel et al., 2022). Suggesting that PL and IL might be important for adapting to changing cues Another study of rats in a trial

unique non-matching-to-location task, found improved performance in the 20s delay condition when ChABC was injected in the mPFC (Anderson et al., 2020). As studies of the mPFC and PNNs have often been conducted based on addiction, few have been conducted based on appetitive-driven motivation alone in learning.

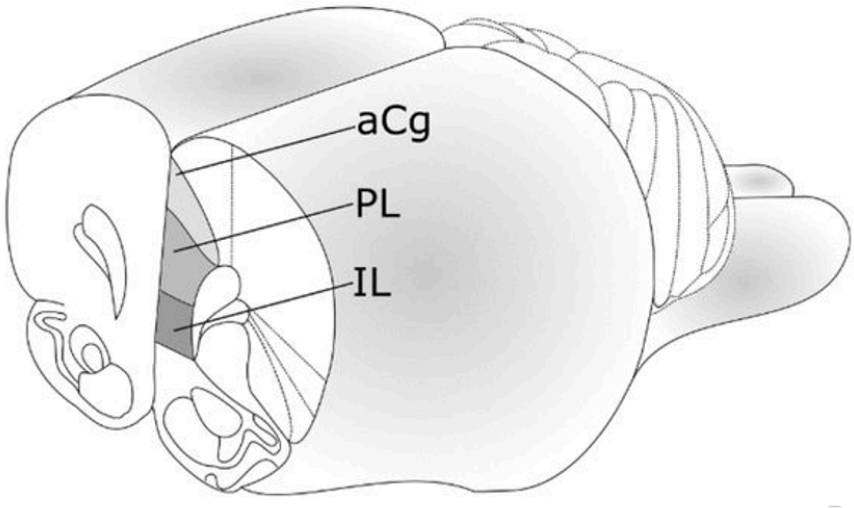

Figure 4: Subdivisions of the mPFC in the rodent brain. Anterior cingulate cortex (aCg), prelimbic cortex (PL) and infralimbic cortex (IL). Adapted from (Domingues et al., 2021).

1.4 Conditional learning

1.4.1 Classic conditioning

Classical conditioning is a form of associative learning in which a formed association alters a behaviour. The most famous example of classical conditioning is the experiment with Pavlov's dogs, in which an association between a bell and food made his dogs start salivating from the bell alone (Pavlov, 1906). The unconditioned stimulus (food) evokes an unconscious or automatic response, referred to as the unconditioned response (salvation). The neutral stimulus (bell) becomes the conditional stimulus, as a learned association evokes a response. The bell's ringing (conditional stimulus) is then associated with the food and elicits the same response as the unconditional stimulus.

1.4.2 Operant conditioning

Operant conditioning builds on the concepts of classical conditioning of a predicative relationship but assesses an active form of learning of voluntary behaviours. This form of learning is also called instrumental learning and was first proposed by Edward Thorndike in his studies of learning in the concept of the law of effect (Thorndike, 1905). In operant conditioning, reinforcement or consequences modify behaviour in a specific direction. This creates an association between the behaviour and the consequence and assesses an active form of learning contrary to classical conditioning (Bear et al., 2001). This type of learning is essential in adapting to our environment as we constantly process environmental stimuli and behave accordingly. Operant conditioning has been widely applied in rodent experiments as it tests various cognitive functions, brain areas and learning (Abela & Chudasama, 2013; Chudasama & Robbins, 2003; Horner et al., 2013). An automated platform of operant conditioning is the touchscreen operant chamber. This highly translational testing method allows for analysing executive functions, motivation and cognitive flexibility with minimal experimenter involvement (Horner et al., 2013; Piiponniemi et al., 2017). A visual discrimination task is one form of learning that can be performed using this platform (Horner et al., 2013). It is a task that tests the animal's ability to visually distinguish between a rewarded stimulus and a stimulus-causing punishment. This stimulus-reward association is learned through repeated training and is appetitively motivated, usually by food restriction. The rewarded stimulus can be reversed to assess cognitive flexibility, as the previously rewarded stimulus is now being punished (Turner et al., 2017). To make this switch, the animals must re-learn the stimulus-reward association and inhibit the previously learned association.

1.5 Methodology

1.5.1 The Adeno Associated Virus (AAV) as a gene delivery system

Previous methods of PNN targeting have harboured some challenges, such as imprecise targeting, short-lasting effects, high cost or being time-consuming. A new method proposed using the adeno associated virus (AAV) for gene delivery targeting PNNs, could solve some of the aforementioned challenges. The AAV has become a well-established viral delivery system for research and clinical trials (Meier et al., 2020). Its genome is fully sequenced and consists of a single-stranded deoxyribonucleic acid (DNA) of approximately 4,8 kilobases containing two genes, rep, and cap,

important for the AAV's essential properties (Aponte-Ubillus et al., 2018). The AAVs genes are flanked by inverted terminal repeats of 145 bases each, leaving everything outside of these repeats excluded from the AAV vector. By replacing the wild-type genome of the AAV inside the inverted terminal repeats, the AAV can be engineered into a highly customisable delivery vector. By depriving the virus of its normal genome, the toxicity and immune response of the virus is lowered. However, the AAV itself cannot replicate without a helper virus such as the adenovirus, making it suitable for *in vivo* use (Kroes, 2010). The recombinant AAVs can be produced by triple transfection using cells, with two plasmids needed for viral production and one hosting the transgene (Challis et al., 2019).

With a single injection the AAV can deliver a long-lasting gene expression, with a variety of genetic input due to its customizability. With around 12 serotypes, differences in the AAV surface proteins, the recombinant AAV can target specific tissues (Li & Samulski, 2020). For example, the AAV2 has been widely used for targeting the CNS locally, while the AAV9 is capable to bypass the blood brain barrier, targeting the CNS from systemic injections (D. Wang et al., 2019). The choice of promoter is also important, as it allows for cell-specific targeting and regulates the level of gene expression. Strong and ubiquitous promoters can be used for overexpression of a transgene, while weaker promoters can be used for a lower level of gene expression.

Some limiting factors are also worth mentioning. The small genome of the AAV naturally limits its packing capacity, excluding the use of transgenes exceeding 5 kilobases. Formation of large transgenes into micro genes, may allow for the viral packaging, but requires in-depth knowledge about the specific gene structure (Wang et al., 2019). Although the AAV is favourable for gene therapy, its effect does not persist, because of its replication-dependency and low frequency integration. To enhance the persistence of the transgene, site specific genomic integration is a good option.

1.6.2 Clustered Regularly Interspaced Short Palindromic Repeats (CRISPR)

Clustered regularly interspaced short palindromic repeats (CRISPR) utilises the immune system of the bacteria *Streptococcus pyogenes*, but has since its discovery become a highly specific gene editing tool (Le Rhun et al., 2019). When a pathogen is encountered, its identification is stored in the memory bank of our immune system. The memory bank expands for every new pathogen encountered, adding up to a wide range of identifications ensuring a stronger immune response upon subsequent infections. For roughly half of bacteria and most archaea, this memory encompasses a specialised DNA sequence in the host genome consistent of CRISPR arrays (Pourcel et al., 2019). The host, harbouring the CRISPR array, stores viral DNA sequences of 30-40 base pairs, called protospacers, from nucleic acid invaders previously encountered. These protospacers are cut by a protein complex of two proteins, Cas1-Cas2, cutting the viral DNA upstream of a protospacer adjacent motifs sequence. The protospacer gets integrated into the host genome as spacer sequences, interspaced by repeat regions downstream of a leader sequence and a promoter. Once an infection has occurred, a ribonucleic acid (RNA) ribonuclease transcribes the CRISPR array into a pre-CRISPR-RNA consistent of a spacer region, parts of the adjacent repeat region and an unprocessed tracer RNA. This tracer region binds to the repeat regions of the CRISPR array. The pre-crRNA sequence, now called a guide RNA, has a unique structure due to the formation of hydrogen bonds between the repeat sequence and the tracer RNA. This structure is necessary for the guide RNA binding to a CRISPR-associated protein called Cas9 disabling the viral DNA by introducing double strand breaks. This guide RNA is exactly what researchers genetically engineer to alter gene expression.

By altering the guide RNA, Jinek et al. (2012) showed that a single guide RNA could be formed by connecting the tracer RNA and pre-crRNA. The simplicity of a two-component system, Cas9 and the single guide RNA, have made CRISPR/Cas9 an efficient and adaptable system for site-specific gene editing. This meant that researchers could direct the Cas9 to all locations in the genome by only changing the spacer region of the single guide RNA. Since then, a variety of uses for the CRISPR system has emerged. CRISPR gene knockout and deletion can exploit the cell's double-strand break (DSB) repair pathway, the non-homologues end joining. Because of the error-prone character of the non-homologues end joining, small inserts or deletions are often introduced at

the break site, which can change the reading frame and cause non-functional genes. Cas9 can also be directed to cause gene flanking DSBs, leading to gene deletion. By homology-directed repair, the other dominant repair pathway of DSBs, a DNA template with the desired gene or sequence, can be implemented into the host DNA to either change, correct or add gene sequences. The homology-directed repair method needs a template to repair DSB and is more precise. For gene editing, this repair template can be engineered to implement the DNA sequence of interest in the location of the DSBs.

1.6.3 CRISPR Activation

In 2013, Qi et al. developed a catalytically dead Cas9 (dCas9) enzyme while maintaining its searching and binding properties. This opened the possibility for site-specific gene repression and activation without altering the DNA sequence, named CRISPRi and CRISPRa, respectively (Figure 5). The principal of CRISPRi was the binding of dCas9 preceding a gene, disrupting transcription factors and RNA polymerase, which resulted in the repression of the subsequent genes. For gene activation, a slightly different technique was used. Transcription activation domains were fused to the dCas9, meaning dCas9 would bring the transcriptional activators to the promotor of the gene, thereby enhancing the transcription (Tanenbaum et al., 2014). The CRISPRa allows targeted gene expression from endogenous loci without inserting exogenous DNA (Heidersbach et al., 2023). Targeting the endogenous genes in an organisms can better our understanding of how the natural processes in the cells work.

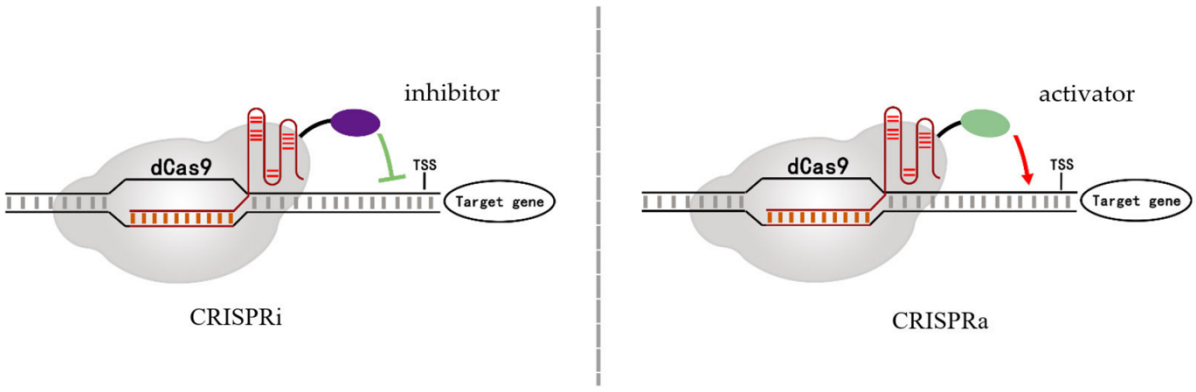

Figure 5: CRISPR inhibition and CRISPR activation using the catalytically dead Cas9. dCas9 binds the DNA preceding the target gene and represses gene expression while CRISPRa activates the expression of the target gene. Figure adapted from (Ding et al., 2022).

1.7 Aims of the study

The PNNs are thought to contribute to the reduced plasticity of the adult brain, supported by solid evidence that removing the PNNs unlocks plasticity in the adult. Periods of heightened plasticity are seen early in development and are important for forming the foundation of neuronal circuits in the brain. As plasticity decreases with age, the neuronal circuits become more stable, and the large reorganisations seen in development do not occur. The exact processes behind the change in plasticity are unknown, but the PNN's role in reducing plasticity has become more evident. Due to limiting methods for PNN targeting, it has been difficult to detangle the exact role of the PNNs, as many methods also influence other elements.

Moreover, the amount of C6 sulphation of the CSPGs is higher in younger animals, indicating its role in the heightened plasticity during development. As the metalloproteinase ADAMTS15 is preferentially expressed in PV cells and is expression is increased during development, these metallopeptidases might play an essential role in the shaping and regulation of the PNNs. In this study, we wanted to perturb genes thought to regulate the PNNs and assess the effect of such perturbations on a behaviour level. We used a new method with viral vectors to target the PNNs more precisely than previously used techniques by exploiting endogenous functions observed in neurons. We hypothesise that a combination of increased C6S and ADAMTS15 can increase plasticity by removing the PNNs, which could in turn, result in faster learning.

The aims of this study include:

1) Pilot a new method of PNN perturbations by using a combination of overexpressing C6ST1 and CRISPR activation of ADAMTS15 delivered through AAVs and assess its effect using immunohistochemical methods.
2) To investigate if the PNN perturbations in the mPFC affect visual discrimination learning.

2. Materials & Methods

2.1 Experimental timeline

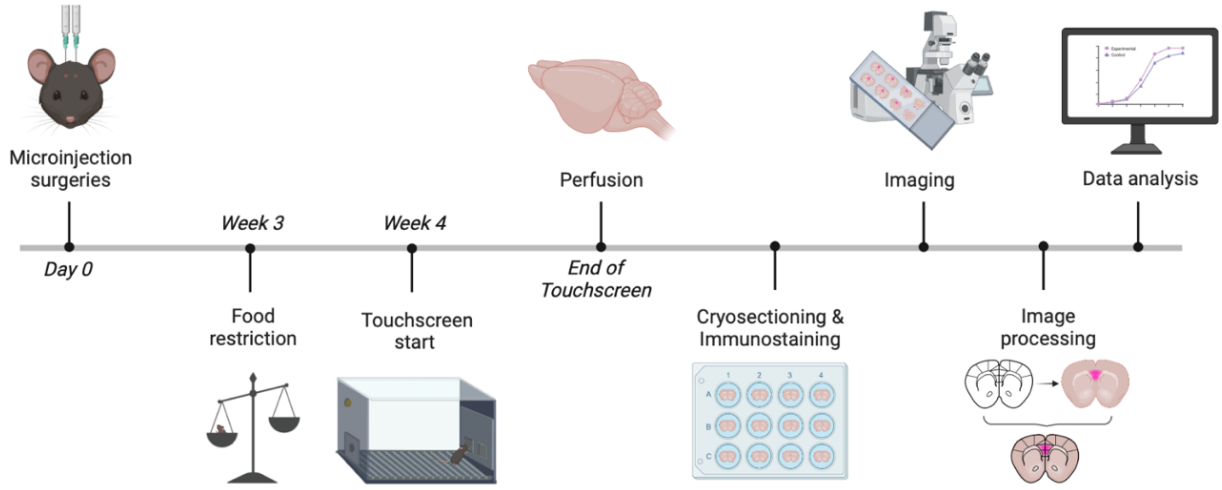

Figure 6: Experimental timeline. Timeline illustrating the procedures of the experiment. Figure created with Biorender.

The events of the experiment illustrated can be seen in Figure 6, starting on the day of surgery. Since each group had several mice, the day of the surgeries within one group was counted as day one. The identity of the viral injections was blinded to prevent potential bias of favouring the experimental group during the behavioural task. After surgery, the mice were housed for four weeks before the behavioural training started to provide sufficient time for viral gene expression. The food restriction started a week before training to motivate the mice for the liquid reward. Once the criterium was met for the last stage of the visual discrimination task, the mouse was sacrificed, transcardially perfused, and the brain was collected. Each brain was sliced, immunostained, mounted on a glass slide and inspected with a microscope. For image processing, dedicated mouse atlases were used, and the site and spread of the injections were analysed. All raw session data from the behavioural task were collected, processed, and distributed into dedicated groups and categories. The data were then analysed and compared to the images to assess the behavioural results concerning the injection location and spread.

2.1 Approvals and experimental animals

All animal experiments and procedures were approved by the Norwegian Food Safety Authority (Mattilsynet, FOTS-approval no. 27415) and conducted according to the Norwegian Animal Welfare Act and European Directive 2010/63. All participants involved in experimental procedures and animal handling held an animal researcher certificate (FELASA C) approved by the Norwegian Food Safety Authority. All animals were housed in the animal facility at the Department of Biosciences, University of Oslo.

A total of 33 animals were used for this study. Three-month-old female C57BL/6JRj mice (n=17, Janvier Labs, France) were bilaterally injected with virus and used for behavioural testing (Supplementary Table 1). Two four-month-old C57BL/6JRj males (n=2, Janvier Labs, France) were used to validate the experimental viruses' separate functions, and six mice were used for surgery training, testing, and refinement of the stereotaxic coordinates. In addition, four female and four male C57BL/6JRj mice (n=8, Janvier Labs, France) were used for a touchscreen pilot project. Animals used to test ADAMTS15 and the C6ST1 virus were housed for four weeks to allow for sufficient viral expression. To minimise the number of animals according to the 3Rs: replacement, reduction and refinement (Russell & Burch, 1959), both experimental viral constructs were tested in the same group of mice instead of having two separate groups. The animals were housed in standard GM500 IVC cages with woodchip bedding (Scanbur A/S, Norway) in groups of three to four. The cages were enriched with nesting material, running wheels/polycarbonate cylinders and softwood (Scanbur A/S, Norway). All cages were housed in a room with a reversed 12-hour light/dark cycle (dark; 12 a.m. - 12 p.m., light; 12 p.m. - 12 a.m.). All testing was performed during the dark period, the active period of the nocturnal mice.

Food restriction was performed to reduce the weight slowly over a week to 85-90 % of their free-feeding weight to ensure motivation for reward during the testing. Food restriction was maintained throughout the behavioural testing until the criteria were met and the tasks were completed. Water was provided *ad libitum.* Each mouse was weighed at a regular time before testing every day. An overview of animals and their inclusion in the statistical analysis can be seen in Appendix A, Supplementary Table 1.

2.2 Surgical procedures

2.2.1 Surgical preparations

Glass pipettes for the microinjection surgery were prepared before surgery started. They were pulled from glass capillaries (0.53 mm I.D., 1.44 mm O.D., 7'' length, Drummond Scientific, USA) in a PP-83 Micropipette puller (Narishige Scientific Instrument Lab, Tokyo, Japan). To get the tip to the desired length, a single layer of soft tissue was used to break the tip and, at the same time, maintain a sharp bevel. The glass pipette was backfilled with rapeseed oil (Eldorado, Norway) and mounted on the Nanoject III (Drummond Scientific Company, PA, USA).

All tools were autoclaved (Enbio S, Enbio Group AG) before the surgeries, and the surgical bench and stereotaxic frame (Model 926, David Kopf Instruments) were cleaned and disinfected with 70 % alcohol. All mice were weighed immediately before the surgery, and syringes with drugs were prepared according to the animal's weight.

2.1.2 Stereotaxic coordinates

Stereotaxic coordinates were found using the mouse brain atlas (Franklin & Paxinos, 2007), as seen in Figure 7B. These coordinates were chosen to increase the probability of targeting the mPFC, as the PL and IL are located along the midline. Coordinates were found using the stereotaxic identification location on the mouse skull, bregma, where the coronal suture cuts the sagittal suture (see Figure 7A). Two rounds of injections were performed using different coordinates. The original coordinates shown in Figure 7B, from the mouse brain atlas, were tested after the second round of surgeries and had to be modified due to differences between the atlas and my measurements. The injections were more posterior, lateral, and ventral than favourable, and the last round's coordinates were adjusted accordingly. The original coordinates were AP 1.8, ML 0.5 and DV -2.5 & -2.0, but had to be modified to AP 2.0, ML 0.4 and DV -2.2 & -1.8. All mice were injected bilaterally at two different depths except for the two mice operated for the separate virus tests.

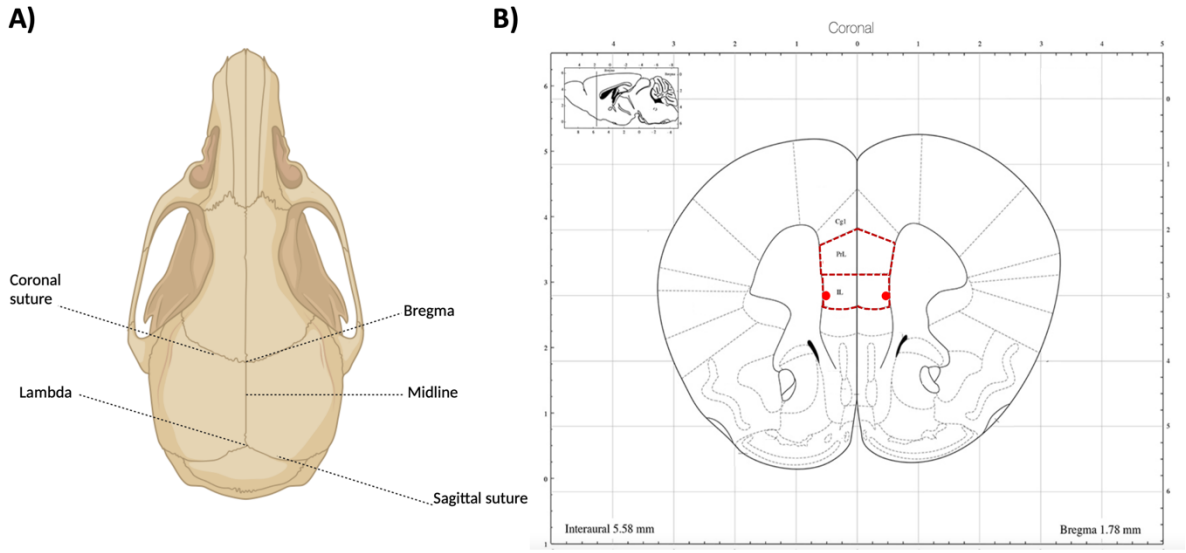

Figure 7: Illustration of the mouse skull with stereotaxic locations, sutures, and coordinates for the microinjections in the medial prefrontal cortex, the prelimbic and infralimbic cortex. **A)** Mouse skull with stereotaxic locations illustrating the positions of bregma and lambda. Created with Biorender. **B)** Coronal view of the mouse brain, with injection coordinates marked with red dots, adapted from (Franklin & Paxinos, 2007).

2.1.3 Viral constructs

All viral constructs were produced by doctoral research fellows Guro Hélen Vatne and Sverre Grødem, following an adapted protocol from Challis et al. (2019).

A 50/50 mix of two viral constructs was used for the experimental group: pAAV-EF1a-C6ST-1-mScarlet (titer: 9.08E+12) and pAAV-SCP1-dSa VPR mini. -2X snRP-1 BsaI gRNA (titer: 3.17E+13) with serotypes AAV9 and PHP.eB, respectively. The promoter human elongation factor-1 alpha (Ef1a), known for its long-term and high transgene expression, was used in the C6ST viral construct, ensuring an overexpression of C6ST1 in the cells infected (Wang et al., 2017). A red fluorescent protein, mScarlet, was linked to the C6ST1 transgene, making the sulfotransferase visible without further immunolabeling.

The CRISPRa construct contains transcriptional activation domains (VPR) fused to dSaCas9, expressed from the SCP1 promoter, in addition to a scaffold with the gRNA sequence

“GCTCTTGCTCAGGAGGCGGGA” to target the transcription start site upstream of the ADAMTS15 gene in mice.

The control group used pAAV-CAG-mNeonGreen (titer: 9.62E+12) with serotype PHP.eB. This viral construct with the chicken beta-actin (CAG) promoter ubiquitously expresses the green fluorescent protein mNeonGreen in the infected cells, visualising the injection sites like the C6ST AAV mentioned.

pAAV-FLEX tdTomato (titer: 1.08E+14) with serotype PHP.eB was a gift from Edward Boyden (Addgene plasmid #28306 http://n2t.net/addgene:28306; RRID: Addgene_28306) and was used to visualise the ADAMTS15 injections.

2.1.4 Microinjection surgery

Animals were anaesthetised with an inhalation anaesthetic, Isoflurane (Baxter, Oslo, Norway) mixed with air. The animals were placed in an induction chamber with 3-4 % Isoflurane until the breathing frequency slowed down. Once anaesthetised, the animals were moved to a heating mat (37 °C) with a gas anaesthesia mask, where the Isoflurane concentrations were lowered to 1.8-2.0%. To establish balanced anaesthesia, an analgesic (Temgesic, buprenorphine, 0.05 mg/kg, Indivor) was injected subcutaneously (sc), and a local anaesthetic (Marcain, bupivacaine, 1-2 mg/kg, Aspen) was injected sc on top of its shaved and disinfected scalp. An anti-inflammatory drug (Dexadreson vet., dexamethasone, 2 mg/ml, MSD Animal Health) was injected intramuscularly into the hind leg to prevent swelling of the brain, and heated Ringer-acetate (Fresenius Kabi AB, Norway) was given to maintain fluid levels. Breathing rate and reflexes (toe pinch and tail pinch) were continuously checked during the surgery.

The animal’s head was fixated on the stereotaxic frame using adjustable ear bars to secure the head and to ensure the skull was levelled. Once secured, an incision was made in the scalp to expose the skull. The stereotaxic identification locations, bregma and lambda, were used to level the head further. Lambda is located posterior to bregma and where the sagittal suture cuts the lambdoid suture (see Figure 7A). The stereotaxic arm was equipped with a needle tip and was used to level bregma and lambda by adjusting the angles for the head. A pen was used to mark

the coordinates once the levelling was 0.3 mm or below. Craniotomies were performed using a handheld dental drill (Perfecta-300, W&H Nordic) with a 0.5 mm drill bit (Hager and Meisinger GmbH). The virus could be injected once the craniotomies were clean and the brain surface visible. Using the Nanoject III attached to the stereotaxic frame, the coordinates were located using bregma as the starting point (Figure 7A). The glass pipette was lowered slowly until it punctured the Dura Mater and was further lowered to the favourable depth, ensuring that the tip did not move horizontally. It was left for one minute before injection and five minutes after, at both depths, before it was carefully extracted. Three hundred nano litres (nl) of virus were injected at an injection rate of 002 at each depth, adding a total of 600 nl per hemisphere. The skull and tissue were cleaned before the incision was stitched up. Animals were kept in a heated cage and monitored closely until awakening post-surgery.

Aseptic techniques were used before, during and after the surgery to minimise the risk of infection.

2.1.5 Post-operative care

A nonsteroidal anti-inflammatory drug, Metacam (meloxicam, 5mg/kg, Boehringer Ingelheim Vetmedica GmbH), was given at the end of the surgery and a minimum of two days post-operative for pain relief. The mice were monitored several times daily during this critical phase to ensure that the animals were healthy and pain-free. A Ringer-acetate solution was given if needed.

2.2 Behavioural Task

A touchscreen pilot was performed in the spring of 2022 for practice. Two additional touchscreen rounds (11.2022- 04.2023) were conducted, and these results were analysed for the current study.

2.2.1 Behavioural apparatus

Eight touchscreen operant chambers (Med Associates Inc., St Albans, USA) were used for the behavioural testing. All chambers were housed in the same room in the same conditions. The touchscreen operant chamber is an automated way of behavioural testing which presents

computer graphical stimuli (Cook et al., 2004; Horner et al., 2013). Each chamber consisted of a steel grid floor, glass walls, a touchscreen, a reward magazine, a house light, a tone generator and a fan; all encapsulated in a light- and sound-attenuating box. The fan in each chamber masked the white noise from the adjacent chambers. The touchscreen displayed the graphical stimuli of vertical and horizontal striped images (Figure 9C), while the liquid reward (Vanilla soy milk, Goodly) collection occurred at the opposite end of the chamber. A signal and magazine light would mark the incoming reward for each correct response. A reward would be presented by lowering the collection arm into soy milk and scooping it up in the container before it was automatically raised into the position in the magazine. For incorrect responses, the house light was lit, and a noise signalled an incorrect response. No reward was given for incorrect responses, and a 5-second delay was added. Infrared beams were present in three different areas: in the magazine, across the middle of the chamber and by the touchscreen, indicating that a response could be recorded without a physical touch.

2.2.2 Behavioural pre-training

Two days before pre-training, the mice were introduced to the liquid reward and weighed in the experimental room for acclimatisation. All experimental mice underwent five different training stage, each adding a new element of knowledge needed for the visual discrimination task (Figure 8). A maximum of ten days was set for all training stages, except for habituation and initial touch, only lasting a day each. An overall criterion for each stage was that all 30 trials had to be completed, and further criteria were added for the later stages.

The initial stage of pre-training was habituation. This stage aimed to accustom the mice to the touchscreen operant chambers to minimise stress and fear for the following training and tasks. Each mouse was left in their respective chamber for 20 minutes, continuously receiving the liquid reward.

After habituating the mice to the chambers, the visual aspect of pre-training started with the second stage, “initial touch”. The visual stimulus, black and white images, were presented in a pseudorandomised order on the touchscreen. A stimulus signal was presented as the image was

touched, and the reward was delivered. If the image was left untouched, a stimulus offset occurred after 30 seconds, followed by a reward. Once the reward was collected, and after an intertrial interval, a new trial could start, and a stimulus was presented on the touchscreen. The correlation of a signal indicating a reward used in this stage follows the principles of Pavlovian conditioning. The second stage was only completed once to avoid the heresy of passively collecting rewards without touching the visual stimulus.

In the third stage, "must touch", a criterion of touching the stimulus is added. This meant that the stimulus remained on the touchscreen until touched, triggering the delivery of the reward. To move on to the next stage, each mouse had to complete must touch within 17 minutes. Another criterium was added for the fourth stage, must initiate, indicative of its name that the mouse itself had to start the trial by poking its nose into the magazine. For the last stage, "punish incorrect", the mouse had to touch the stimulus image. If it touched outside the stimulus window, it was counted as an incorrect response and a bright light was lit. This stage was included to introduce the mice to punishment for incorrect responses. Each mouse had to reach a criterion of 80% correct responses in two consecutive days to end their training period.

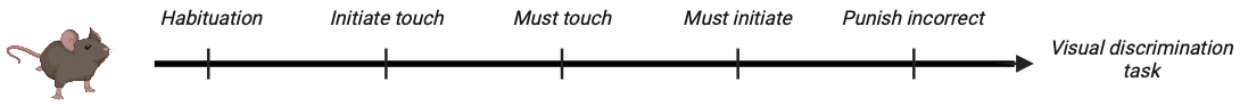

Figure 8: Pre-training timeline. Timeline of stages in the visual discrimination pre-training. The animals were first habituated to the chambers before learning the fundamentals of the visual discrimination task, such as touching stimuli and collecting rewards, in a step-by-step manner.

2.2.4 Visual discrimination task

The visual discrimination task started after completing the "punish incorrect" stage. The stimulus was unintentionally not counterbalanced according to the groups, as most controls started with the same stimulus. At the start of each trial, the magazine light was illuminated, and a reward was given. Each mouse had to initiate the trial by poking its head in the magazine. Once initialised, the stimuli were presented and remained until a response was recorded. If a correct response was recorded, a complete session trial was counted, and the reward was given following a 20s

blackout (Figure 9A). If an incorrect response was recorded, the subsequent trial was a correction trial, not counted as a session trial (Figure 9B). The correction trials mirrored the last position of the stimuli and persisted until the correct response was recorded. The stimuli used and the flow chart of the task can be seen in Figures 9C and D. The correction trials were used to avoid a side bias strategy of only touching the stimulus on one side, which would result in 50% correct responses. For this reason, the stimulus was presented in a pseudo-random order in the standard trials, ensuring that the stimuli were presented equally on each side. Once a correction trial was complete, the initial incorrect response would be counted towards the session's 30 trials. The correction trials were added to the total trials, not to be mistaken with the 30-session trials. The session was finished once 30 trials were complete or 60 minutes had passed. Equal to “punish incorrect”, a criterium of 80% in two consecutive days (only session trials) was needed to complete the task acquisition. Surpassing the chance level of 50%, a success rate of 80% implies an understanding of the task. Animals were moved to the next stage after completion.

The last stage of the visual discrimination task was the reversal acquisition. This stage was identical, except for a reversal of the correct stimulus. The same criteria were used for this last stage, and a maximum of 25 days was set for each visual discrimination task. The reversal task was interesting to conduct as the mPFC is thought to be involved in cognitive flexibility (Turner et al., 2017b).

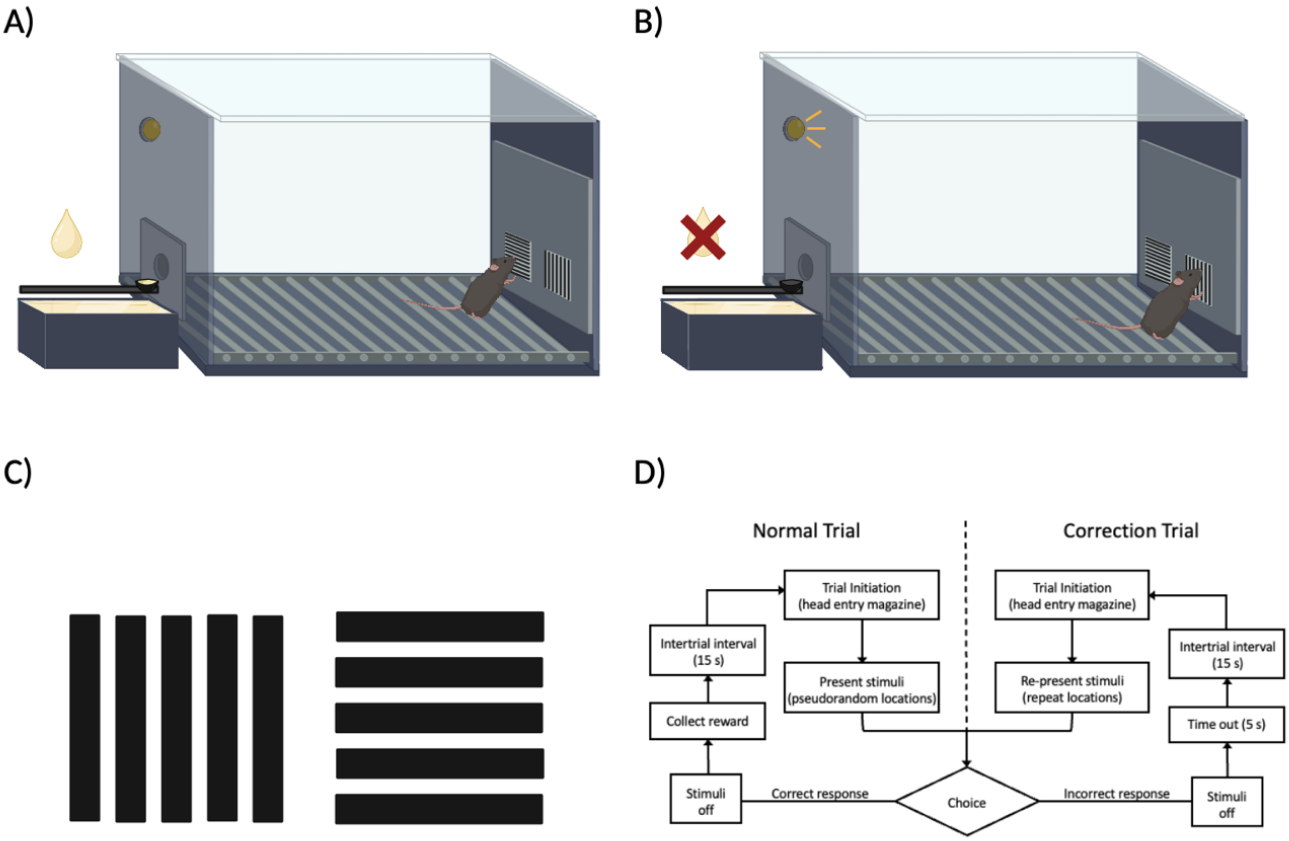

Figure 9: **Correct and incorrect responses, stimuli, and flowchart of the visual discrimination flow chart**. The visual discrimination task in the touchscreen chamber. **A)** Correct response to stimulus delivers soymilk reward. **B)** Incorrect response to a stimulus: The house light (punishment) is lit, and no reward is delivered. **C)** Stimuli. Created with BioRender. **D)** Flow chart adapted from (Horner et al., 2013).

2.2.3 Stimuli

The stimuli used in the visual discrimination tasks were vertical and horizontal black-striped images (Figure 9C).

2.3 Histology

2.3.1 Transcardial perfusion

The mice received an intraperitoneal injection with an overdose of ZRF Cocktail (3.3 mg Zolazepam, 3.3 mg Tiletamine, 0.5 mg Xylazine & 2.6 µg Fentanyl per ml 0.9% NaCl, 0.1 ml/10g) at a concentration of 0.05-0.1 ml/10 g body weight. Reflexes (tail pinch reflex & pedal withdrawal

reflex) were checked before perfusion started to ensure the mice were deeply anaesthetised. Once anaesthetised, the mouse was moved to a fume hood, and a chest incision was made to open the thorax and expose the heart. The right atrium was cut once the heart was fully exposed, and the needle was inserted into the left ventricle. The mice were then perfused transcardially with 10 ml 1X M phosphate-buffered saline (PBS) followed by 4 % paraformaldehyde solution (PFA) until the fixation tremors disappeared (~10 ml) to fixate the brain. The brains were carefully extracted and placed in 4 % PFA solution for 24 hours at 4°C. To prevent the tissue from freezing damage, the brains were transferred to a cryoprotective 25 % sucrose solution (2.5 g sucrose in 10 ml 1X PBS) for 24 hours at 4°C. Brains were stored in plastic bags at –80°C.

2.3.2 Cryosectioning

Brains were thawed at –20°C for +/- 30 minutes in the cryostat (CM1950, Leica Biosystems). To make the brain sections even, each brain was cut above the cerebellum before being placed perpendicularly on the platform and flash-frozen with OCT mounting media (Avantor, VWR Chemicals, Pennsylvania, USA) in the cryostat. The brains were mounted in the cryostat and sectioned into 40 µm coronal sections at - 18-19°C.

2.3.3 Immunostaining of free-floating sections & mounting

To investigate the PNNs, fluorescent immunohistochemical labelling was performed. The injections were visible without further antibody staining since the control virus and the C6ST1 expressed fluorescent proteins. The expression of ADAMTS15, however, was not linked to a fluorescent protein, and additional immunostaining was necessary. Coronal sections were placed in 24 well culture plates free-floating in 1X PBS. All sections were washed 3 x 5 minutes before being placed in a blocking solution to prevent background signals and false positives. The sections were left in blocking for one hour at room temperature on a platform shaker at ~150 rpm. The sections were incubated in primary antibody solution overnight (19-24 hours) at 4°C and in secondary antibody solution for 1-4 hours at room temperature. Primary solutions containing antibodies for WFA, C6S, ADAMTS15, aggrecan, versican, tenascin-R and cas9 were used to stain PNNs and to check or detect the effect of the viral injections (Appendix B, Supplementary table 3). Nissl staining (Neurotrace^{TM} 435/455, Invitrogen, Thermo Fisher, Norway) was added to the

secondary antibody solution and stained Nissl bodies in the neuron's soma. Sections were washed 3 x 5 minutes between primary and secondary antibody solution before mounting the sections on Superfrost plus glass slides (Thermo Fisher Scientific, Oslo, Norway). Sections were allowed to dry completely before being rinsed in MilliQ water to remove excess salts from the PBS. When dry, FluorSave mounting media (Sigma-Aldrich, Darmstadt, Germany) was added to each section, covering it completely, before attaching the cover glass slide. Each slide was washed in ethanol and dried with lens paper.

Since the FluorSave was not wholly air-tight, xylene and entellan were used as mounting media for the last batch of slides (Protocol in Appendix D).

2.4 Imaging

Imaging was performed on an Andor Dragonfly spinning disc confocal microscope (Oxford Instruments, United Kingdom) with a Zyla 4.2 sCMOS (2048 x 2048-pixel, Oxford Instruments, UK). Kristin Larsen Sand acquired overview images with a ZEISS AxioScan Z1 slide scanner at the Institute of Basic Medical Sciences, University of Oslo. The images were acquired with an Orca Flash 4.0 camera (Hamamatsu Photonics, Japan) and a 20x Plan-Apochromat objective (NA 0.8, WD 0.55, Zeiss Microscopy, Germany). Close-up images were acquired using a 40x oil objective (Nikon CFI PlanFluor 40x, numerical aperture of 1.3, working distance of 0.2 mm). Diode laser lines with wavelengths 405 nm, 488 nm, 561 nm and 637 nm were used. Image processing of the overview/close-up images was performed using ImageJ/FIJI Field (Schindelin et al., 2012). The wide scan image processing was performed using the Zen Light software (Carl Zeiss, Oberkochen, Germany). Coronal sections were aligned with the Allen mouse brain atlas to assess the location of the brain area borders and the injection sites.

2.5 Post-processing of images

To validate the spread of the microinjections, the Quint Workflow was implemented. The Quint Workflow consists of several open-source software programs, allowing for efficient pre-processing, aligning each section image, and assessing the spacing between each section (Yates et al., 2019). All images had to go through a pre-processing stage consisting of renaming, rotating,

and sorting before being resized to a width of 1500 pixels using the software Nutil Transform. An XML file had to be created before loading into QUICKNII to align each section to a reference atlas. A JSON file created from QUICKNII was loaded into Visualign, and non-linear adjustments for each atlas were made to fit the respective brain section. Superimposed atlases could be exported and edited in ImageJ to detect edges and remove backgrounds.

2.6 Data and Statistical Analysis

Data for each behavioural session was automatically saved in the K-Limbic system of the touchscreen operant chamber (Med Associates Inc., Fairfax, USA). This raw data was then pre-processed by manually extracting data from each mouse directed into new respective files for all session days in Excel (Microsoft, USA). The relevant data from these files was filtered and adapted through a custom-made Python script made by previous employees in the research group and manually sorted before being exported to GraphPad Prism 9.3 (GraphPad Software Inc., USA). GraphPad prism was used to conduct all statistical analyses and to create figures. Each dataset was assessed for normal distribution by visually inspecting the data in Q-Q plots and with a normality test. Since the datasets varied in normality, unpaired parametric t-tests were used for the normally distributed datasets and Mann Whitney U test for non-normal distributions. A p-value of 0.05 was set as the significance level.

3. Results

The results are divided into two parts. The first part displays the histology, and the second part presents the results from the visual discrimination task.

A total of 33 animals were used for this study. Seventeen mice conducted the visual discrimination task and reversal. One control mouse was not included in the statistical analysis, as it did not complete task acquisition or progress in the reversal acquisition. Two mice were used for separate injections of C6ST1 and ADAMTS15 and are included in the histological results.

3.1 Part 1: Histology

3.1.1 Injections targeting the mPFC

The viral injections were visualised through the fluorescent protein mScarlet linked to the C6ST1 enzyme as the ADAMTS15 had no fluorescent marker. Several attempts were made to visualise the viral gene expression of ADAMTS15 through labelling with antibodies, but these attempts were unsuccessful. As a last attempt, we stained for the Cas9 protein, but no signal was detected. The viral injections could be observed in the mPFC of all animals, but the injections were not restricted. The virus had spread to both anterior and posterior areas from the injection sites. Brain sections from two animals representing the spread are seen in Figure 10. To assess the success of the injections in targeting the mPFC areas PL and IL, all brain sections were analysed with superimposed atlases. Brain sections were visually inspected, and viral expression in the regions of PL and IL was counted as a hit. The injections targeting PL and IL resulted in four bilateral hits, three with a mix (IL on both hemispheres and PL in one), and two unilateral for the experimental group. The mice respective to the different groups and viral expression in other areas are reported in Appendix A, Supplementary Table 2. The full range of the injections according to anterior-posterior positions was not fully mapped as the tissue sampling was performed around the target area, and the viral injections had spread further beyond this point. It also seemed like some of the viral injections had entered the ventricles, broadening the spread of the virus (Figure 10Aiii+Biii).

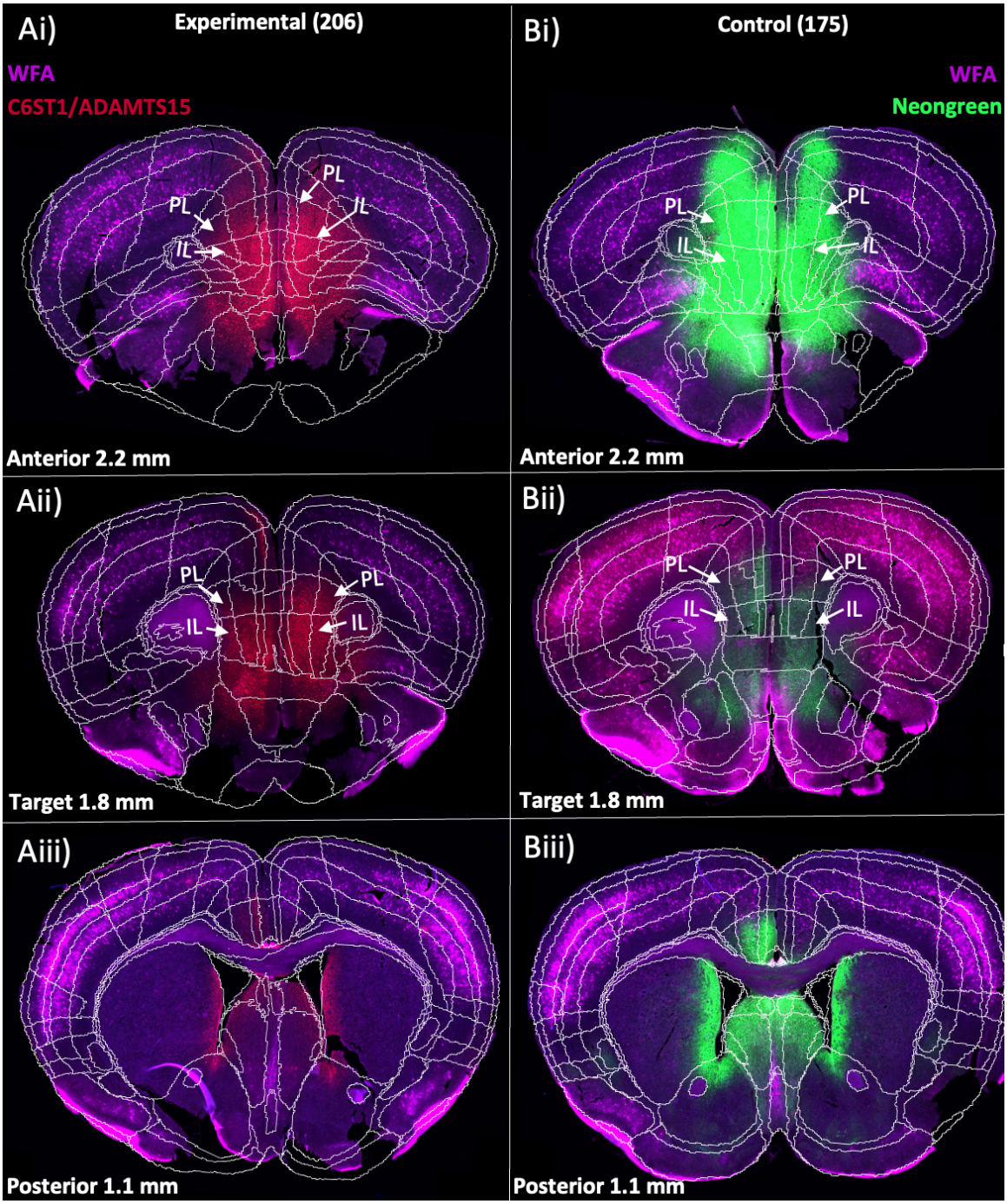

Figure 10: Target site and typical spread of viral injections of C6ST1/ADAMTS15 and control. Experimental and control brain sections display the most anterior section to the most posterior, with the target site in the centre. All brain sections are superimposed with custom atlases and stained with WFA in Far red (pink) to visualise the PNNs. Injection sites were displayed as red for the experimental group and green for the controls by the linking of fluorescent proteins mScarlet and Neongreeen, respectively. Target areas are marked PL (prelimbic) and IL (infralimbic). **Ai)** The most anterior brain section of experimental mouse 206. **Aii)** Brain section around the target area. **Aiii)** The most posterior brain section. **Bi)** The most anterior brain section of the control mouse 175. **Bii)** Brain section around the target area. **Biii)** The most posterior brain section.

3.1.2 A reduction in WFA with the combined C6ST1 and ADAMTS15 overexpression

After evaluating the distribution of injections, a thorough examination of their effect of overexpression on the PNNs was conducted. WFA was used to inspect the PNNs. For the viral combination C6ST1/ADAMTS15, a reduction in WFA staining was observed around the injection sites (Figure 11Ai-iii). This reduction was not seen for the control group (Figure 11Bi-iii). To assess whether the decrease of WFA was a result of the combination of C6ST1 and ADAMTS15 or could be caused by their separate function, two unilateral injections were performed for the individual viruses in two animals (301 ADAMTS15 and 302 C6ST1). To visualise the injection site and virus spreading, an AAV virus expressing the red fluorescent protein TdTomato was mixed with the ADAMTS15 virus. The ADAMTS15 viral injection did not show a reduction in WFA staining (Figure 11Ci-iii), while the C6ST1 showed a slight decrease in WFA staining (Figure 11Di-iii).

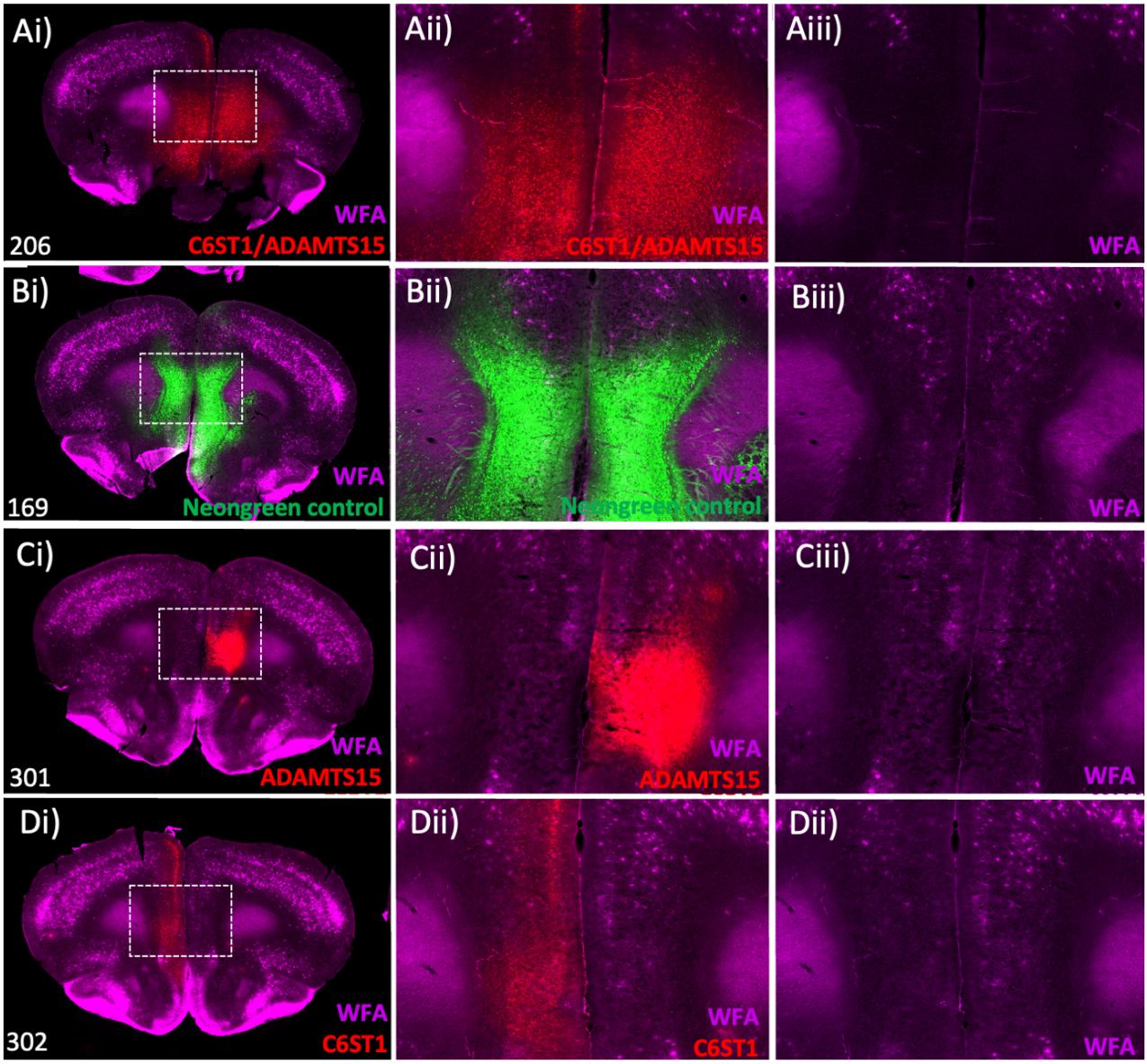

Figure 11: WFA staining of the PNNs around the injection sites for the C6ST1/ADAMTS15 combination (206), control (169), ADAMTS15 (301) and C6ST1 (302). Brain sections were stained with WFA (pink), and the viral injections were visualised from the different fluorescent proteins (red or green). **Ai)** Overview picture of mouse 206 and with the C6ST1/ADAMTS15 combination injection. **Aii)** Close-up of the mPFC with viral injection and WFA staining. **Aiii)** Close-up of the mPFC with viral injection and WFA staining. **Bi)** Overview picture of mouse 169 and with the Neongreen control injection. **Bii)** Close-up of the mPFC with viral injection and WFA staining. **Biii)** WFA staining of the mPFC. **Ci)** Overview picture of mouse 301 and with the ADAMTS15 injection. **Cii)** Close-up of the mPFC with viral injection and WFA staining. **Ciii)** WFA staining of the mPFC. **Di)** Overview picture of mouse 302 and with the C6ST1 injection. **Dii)** Close-up of the mPFC with viral injection and WFA staining. **Diii)** WFA staining of the mPFC.

3.1.3 No aggrecan staining in the mPFC of C6ST1/ADAMTS15 or controls

Since WFA staining does not stain all PNNs, it was important to stain other components of the PNNs. Aggrecan, an abundant lectin component of the PNNs, were stained using an aggrecan antibody (ACAN) to visualise PNNs not stained by WFA. The aggrecan antibody only stained a few PNNs at the bottom of each section around the substansia insomiata and nucleus accumbens, indicating that the staining did not work for the desired population of cells (Figure 12A+E). No aggrecan was observed in the mPFC or around the injections in either the experimental group (Figure 12B-D) or the controls (Figure 12F-H). Immunostaining of other PNN components like versican and tenascin-R were performed but did not work.

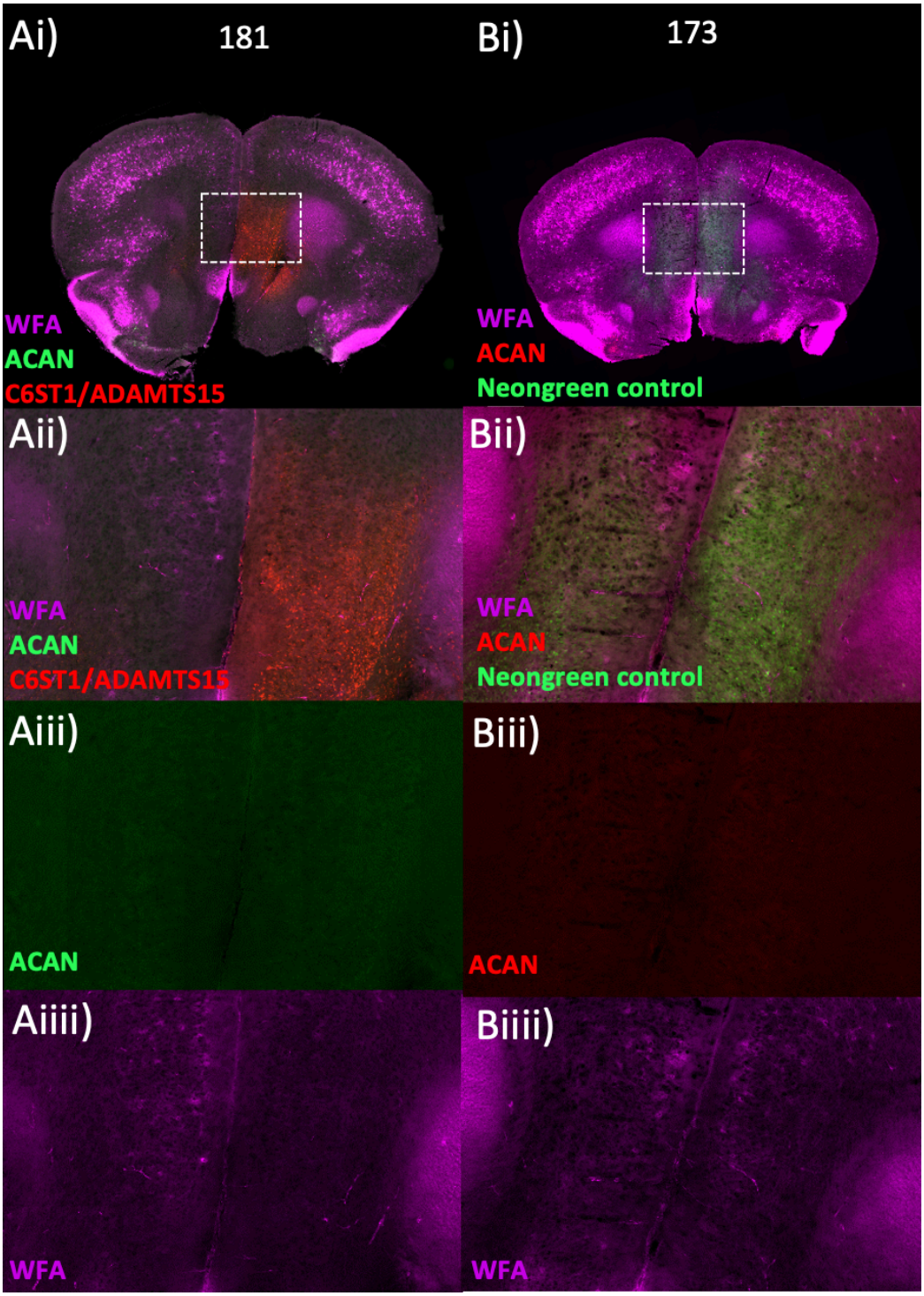

Figure 12: WFA and aggrecan staining of the PNNs around the injection sites for the viral combination (181) and control (173). Brain sections were stained with WFA (pink) and aggrecan (ACAN), in green for the experimental animals and red for the controls. **Ai)** Overview picture of experimental mouse 181 with the C6ST1/ADAMTS15 combination injection. **Aii-iii)** Close-up image of the mPFC with WFA (pink) and aggrecan staining (green). **Bi)** Overview picture of control mouse 173 with the Neongreen injection. **Bii-iii)** Close-up image of the mPFC with WFA (pink) and aggrecan staining (red).

3.1.4 C6S staining found in both the C6ST1/ADAMTS15 combination and C6ST1

To see whether the expression of the C6ST1 resulted in C6 sulphation in the PNNs, staining of C6S was performed on brain sections of mice from all the different virus combinations (Figure 13). Staining of the C6S was observed around a few cells in the C6ST1/ADAMTS15 combination (Figure 13Ai-iii) but not in the controls (Figure 13Bi-iii). Proper quantification is necessary, but visual inspection suggests that no C6 sulphation was observed in either the controls (Figure 13Ci-iii) or the ADAMTS15 mouse (Figure 13Di-iii).

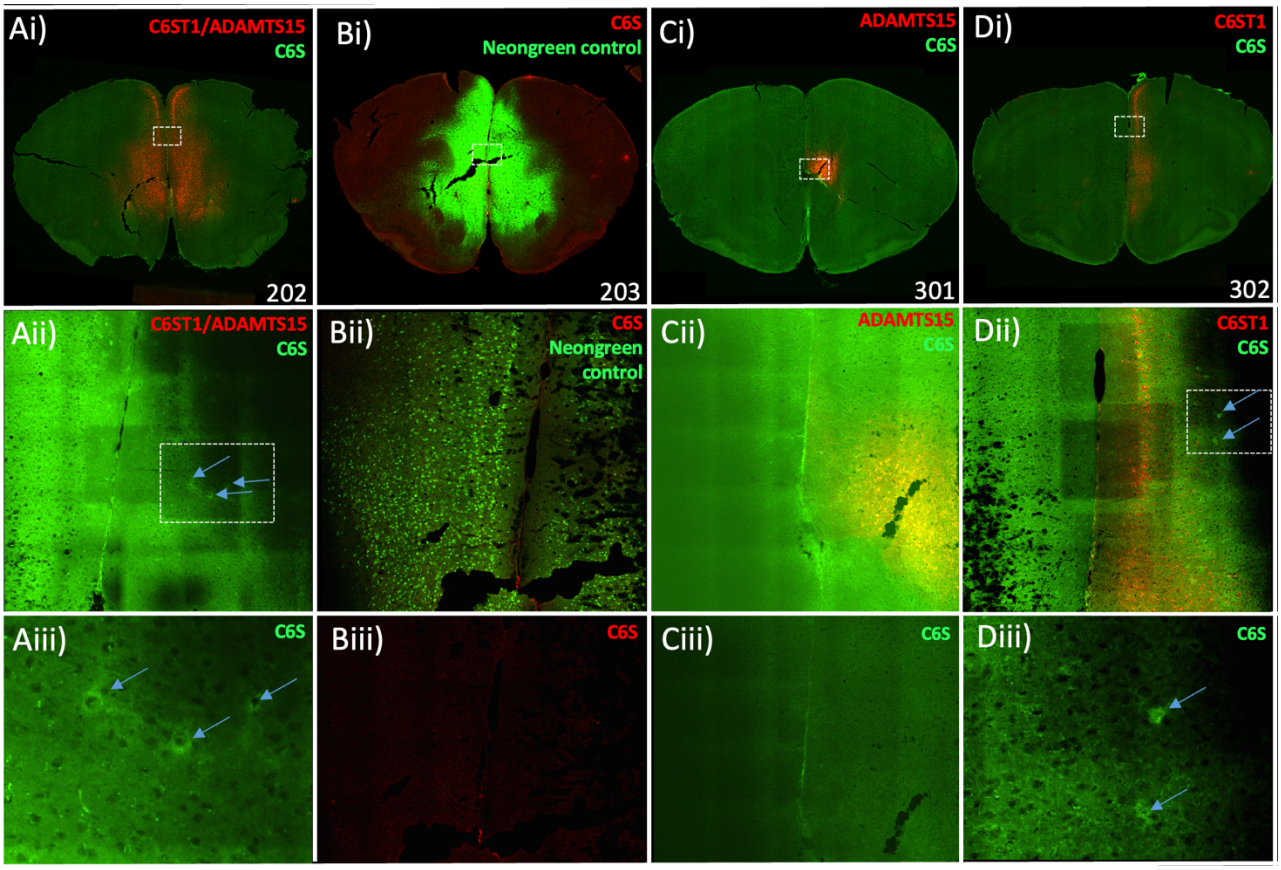

Figure 13: Staining of C6 sulphation of mice with the C6ST1/ADAMTS15 combination (202), Neongreen control (203), ADAMTS15 (301) and C6ST1 (302) injections. Ai) Overview image of mouse experimental mouse 202 with C6ST1/ADAMTS15 combination injection. **Aii-iii)** Close-up image around mPFC. **Bi)** Overview image of control mouse 203 with Neongreen injection. **Bii-iii)** Close-up image around mPFC. **Ci)** Overview image of mouse 301 with ADAMTS15 injection. **Cii-iii)** Close-up image around mPFC. **Di)** Overview image of mouse 302 with C6ST1 injection. **Dii-iii)** Close-up image around mPFC. Close-up images were acquired using a CFI Plan Fluor 40x/1.3 NA objective.

3.2 Part 2: Behavioural task

One mouse from the control group (201) was excluded from all statistical analysis because it failed to complete task acquisition and showed no progress in the reversal task. The behaviour results were firstly divided into subgroups corresponding to viral vector hits into mPFC (Appendix A, Supplementary Table 2). Due to few animals in each subgroup and only two in unilateral, the experimental was kept as one group for the statistical analyses of the behavioural results. The individuals in each subgroup were marked with different colours for all bar plots to display differences.

3.2.1 Similar results were seen when dividing the groups based on injection success

A selection of plots is presented in this section to assess whether differences in injection success affected the performance in the visual discrimination task. Since the unilateral and mix groups did not have the complete viral injections in mPFC, they did not have the full treatment. T-tests comparing the bilateral and controls were performed to check for treatment effects.

A significant difference in the days until criterium was seen for the bilateral group in the reversal acquisition (unpaired parametric t-test, $t(9) = 3.855$, p-value = 0.0039), but not for task acquisition (unpaired parametric t-test, $t(9) = 0.1648$, p-value = 0.8728). All groups spent a similar number of days on task acquisition (Figure 14A). A larger variation was seen for the reversal acquisition for both bilateral and mix. In contrast, a clustering of data points was seen towards the cut-off day for both controls and unilateral (Figure 14B). One mouse in the unilateral group and three in the control group did not complete reversal acquisition.

All groups displayed similar trends at the start of task acquisition (Figure 14C). The percent correct choices for the bilateral, mix, and controls had similar trends, while the unilateral had, on average lower scores mid-task. Only one mouse was left in the unilateral group towards the end of task acquisition and reversal.

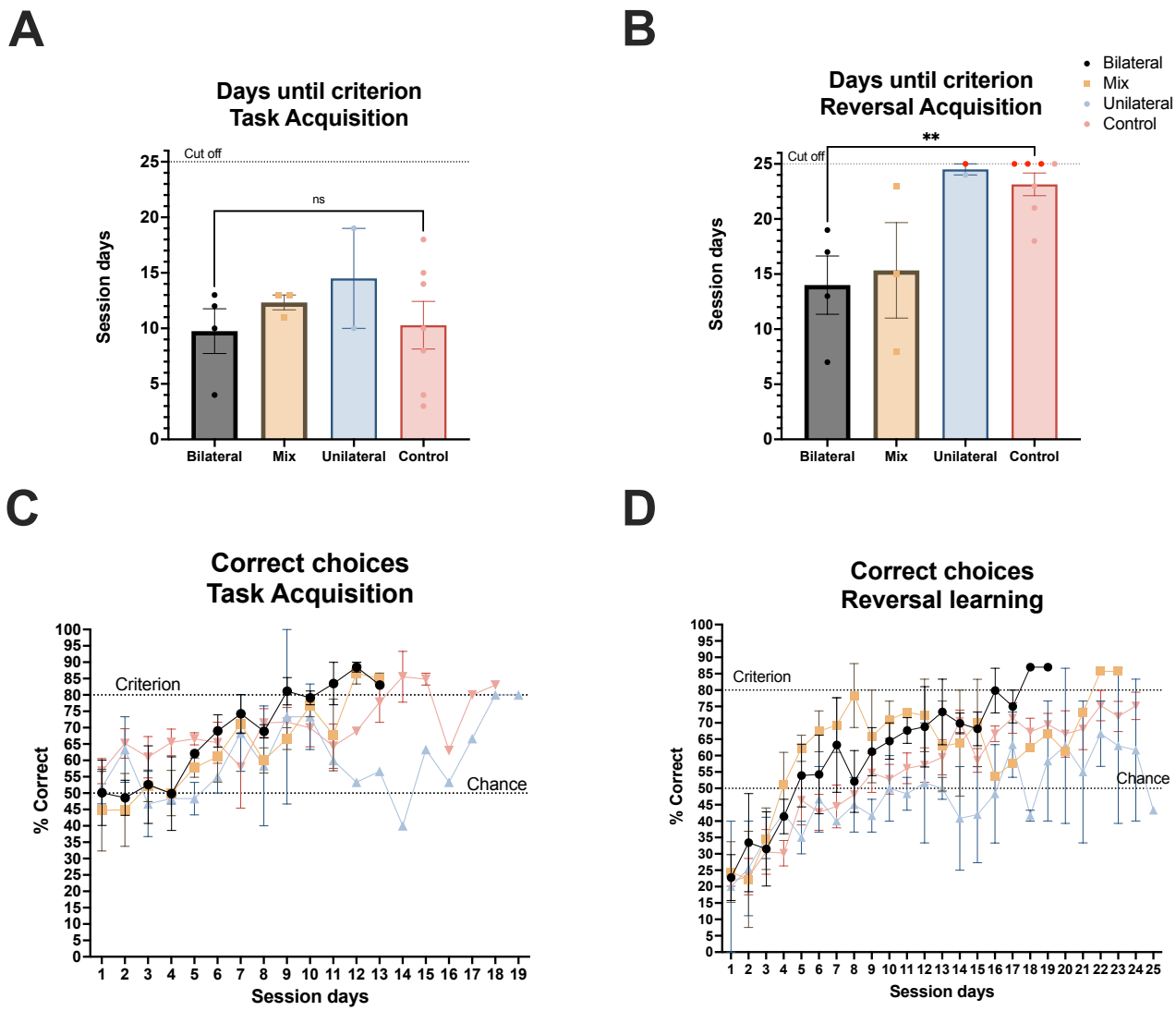

Figure 14: Days until criterion and correct choices for the divided groups. The plot displays the number of days until criterion and percentage correct across session days for bilateral (n=4), mix (n=3), unilateral (n=2) and control group (n=7). The plots present the mean ± SEM. **A)** Days of task acquisition, measured by unpaired parametric t-test, p value = 0.8728. **B)** Days of reversal acquisition, measured by unpaired parametric t-test, p value= 0.0039, $p < 0.01$ is indicated by ** **C)** Correct choices in task acquisition **D)** Correct choices in reversal acquisition.

3.2.2 Days of task acquisition were similar but C6ST1/ADAMTS15 spent less days on reversal acquisition

The number of days needed to reach the criterion was treated as a general measure of learning, as less days implicates better learning of the stimulus-reward association (Van Den Broeck et al., 2019). Both groups acquired task acquisition within 25 days and no significant difference was seen between the groups (unpaired parametric t-test, t(14) = 0.5755, p-value = 0.5741). A larger variation could be seen for the control group, while a clustering around day 10 to 13 was seen in the experimental group (Figure 15A).

For reversal acquisition, the experimental group used fewer days to reach the criterion compared to the controls (Mann-Whitney U test, p-value = 0.0308) (Figure 15B). The shortest time spent for the control group was 18 days, while most animals in the experimental group completed the reversal acquisition before this day, with the fastest completing in 7 days. A larger variation in the experimental group could be seen, while the controls clustered around the cut-off. Three mice from the control group and one from the experimental group were not able to complete the task in 25 days and were stopped after the session on day 25 (Figure 15B, red dots).

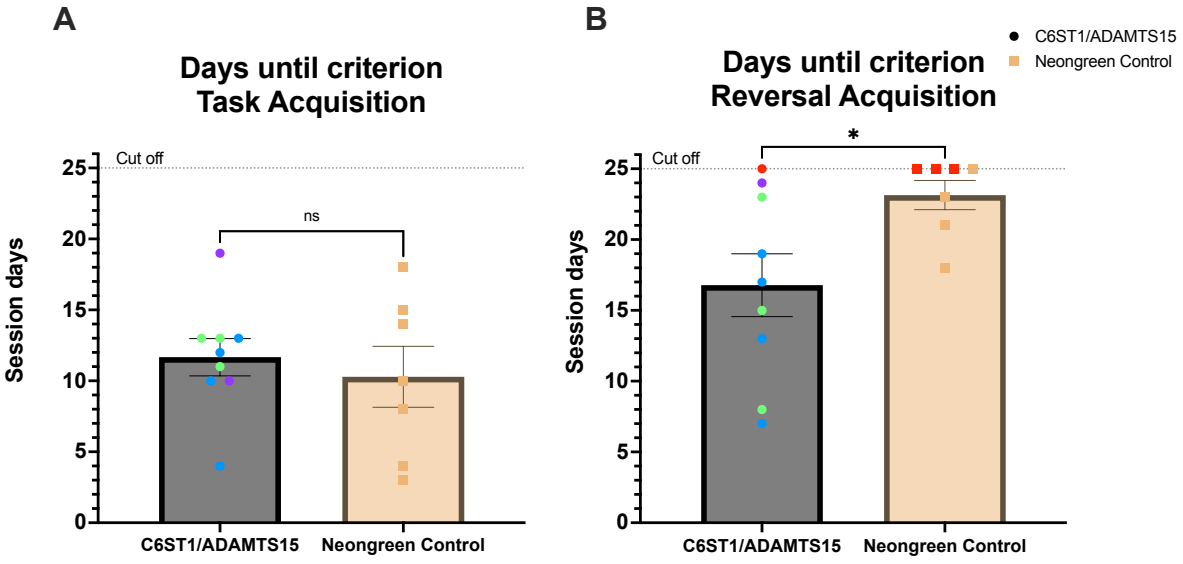

Figure 15: Number of days spent until completion for both task and reversal acquisition. Each dot represents the total number of days each mouse spent to achieve the 80% criteria for experimental (n=9) and control group (n=7). The dots are divided into different colours based on the injection's success. Blue dots indicate a bilateral

injection of PL and IL, green dots for unilateral + IL on the other hemisphere (mix), and purple for unilateral. Mice unable to complete the task before the cut off day are marked as red dots. The bar plots present the mean of both groups and are presented with the standard error of the mean (SEM). The dotted line represents the cut off day for each task. A) Days of task acquisition, measured by unpaired parametric t-test, p-value = 0.5741. B) Days of reversal acquisition, measured by Mann-Whitney U test, p value= 0.0308, p < 0.5 is indicated by *.

3.2.3 Both experimental and control animals displayed similar trends in correct choices

After analysing the number of days required, the progression of performance (percent correct choices) was assessed (Figure 16A+B). Both groups started out around chance for task acquisition, but the control group performed better in the first days. However, the performance started to even out during the course of the task. The lower performance scores towards the end for both groups are due to few animals left.

For the reversal task, the performance of the experimental group was slightly better than for the controls (Figure 16B). Both groups showed a similar trend of around 20% correct on the first day. After day three, the experimental group showed higher percent correct choices values until day 14, where the scores became more similar of around 60-70%.

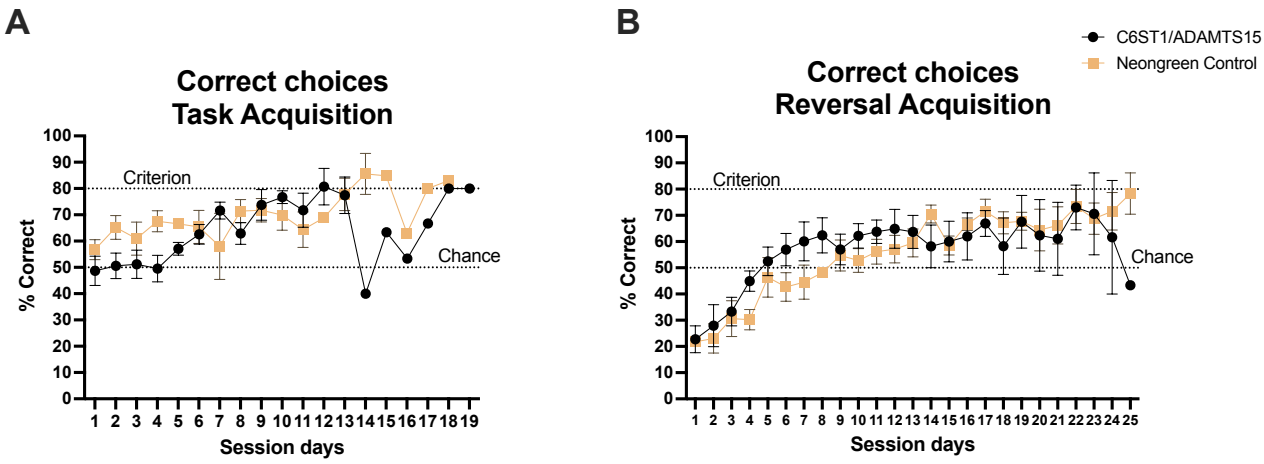

Figure 16: Correct choices of both groups across the session days for task acquisition and reversal acquisition. The correct choice score displays the number of correct responses in each session. The data presents the mean ± SEM of both experimental (n=9) and control group (n=7) across session days. The lower dotted line represents chance level (50%) and the upper line represent the criterion level (80%). **A)** Correct choices in task acquisition **B)** Correct choices in reversal acquisition.

3.2.4 The experimental group spent more time during task acquisition

The amount of time spent per trial was analysed and the experimental group spent significantly more time during task acquisition compared to the control group (unpaired parametric t-test, t(14) = 3.315, p-value = 0.0051) (Figure 17A). When assessing the progression of time spent across the consecutive session days, the experimental group spent more time during the entire experiment than the controls (Figure 17B). In the reversal acquisition, no difference was observed between groups (unpaired parametric t-test, t(14) = 0.1093, p-value = 0.9145) (Figure 17C). When assessing the time across sessions, a decrease in time was seen during the start of reversal for both groups (Figure 17D).

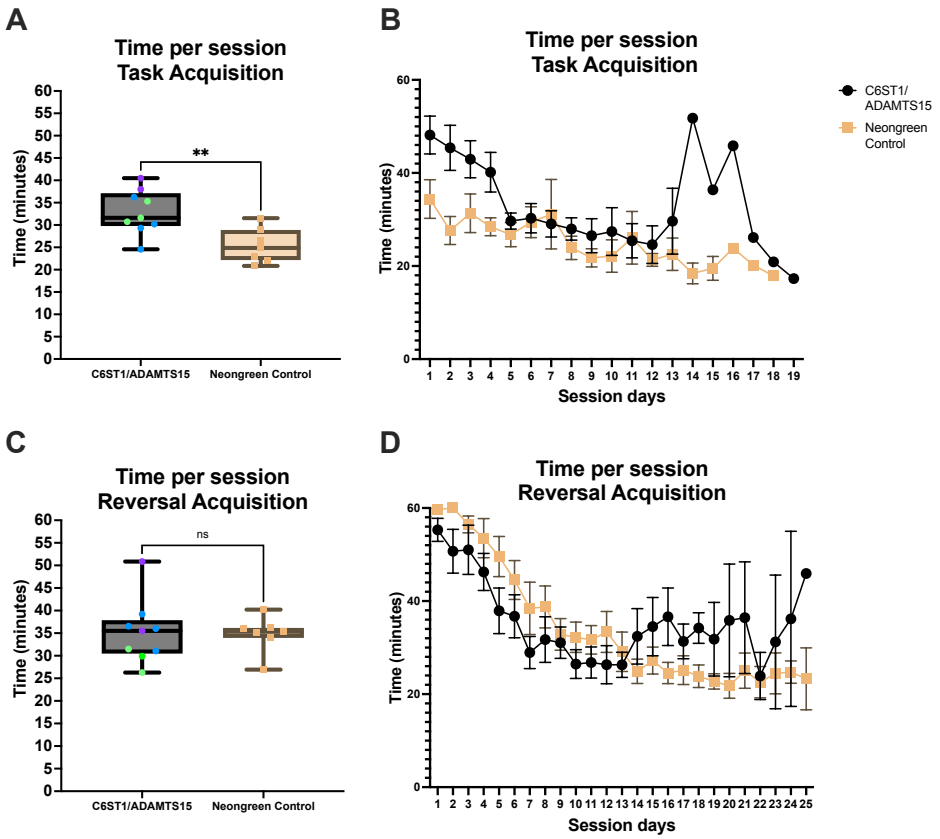

Figure 17: Time spent per session on task acquisition and reversal acquisition. Each dot represents the average time each mouse spent during the sessions. Blue dots indicate a bilateral injection of PL and IL, green dots for unilateral + IL on the other hemisphere (mix), and purple for unilateral. XY plots are presented as mean ± SEM. Boxplots display the minimum and maximum values, first and third quartile and the median**. A)** Session time for each individual mouse in task acquisition, measured by unpaired parametric t-test, p-value=0.0051. P < 0.01 indicated by **. **B)** Time spent during the sessions over the course of days for both groups for task acquisition. **C)** Reversal acquisition, measured by unpaired parametric t-test, p-value = 0.9145. **D)** Time spent during the sessions over the course of days for both groups in reversal acquisition.

3.2.5 A larger variation in response latencies for the experimental group

To assess motivation in relation to the reward, parameters of reward collection, trial initiation and total latencies were analysed. Reward collection latency displays the time to collect a reward after touching the correct stimuli. Both groups started out with similar latencies for reward collection in task acquisition (Figure 18A). An increase in the latency was seen for the experimental group midway, while the controls had similar values. The reward collection latencies for reversal started similarly as task acquisition (Figure 18B). Moreover, the controls displayed a constant trend with a slight increase towards the end, while the experimental groups spent a bit longer collecting the rewards. To assess whether the weight of the animals could explain these differences, tests were performed to check for weight differences between the groups (Appendix C, Supplementary Figure 1). No significant difference in weight was seen between the groups in task acquisition (unpaired parametric t-test, $t(14) = 0.3094$, p-value = 0.7616) or in reversal acquisition (Mann-Whitney U test, p-value = 0.5360).

Trial initiation is the time spent initiating a new trial. In task acquisition, both groups started out with similar latencies, but the experimental group spent longer initiating the trials after day 6 (Figure 18C). The controls displayed a more constant trend in trial initiating (Figure 18D). For reversal, the control group seemed to be slower to initiate the trials compared to the experimental in the beginning, and a peak was seen around day 3. The experimental group displayed a peak after day 14, where they were slower to initiate until both groups spent less time initiating the trials towards the end.

Total latency illustrates the time spent to decide between stimuli. A slight downward slope towards less time choosing across days was seen for task acquisition (Figure 18E). The controls spent longer deciding at the reversal start than the experimental animals (Figure 18F).

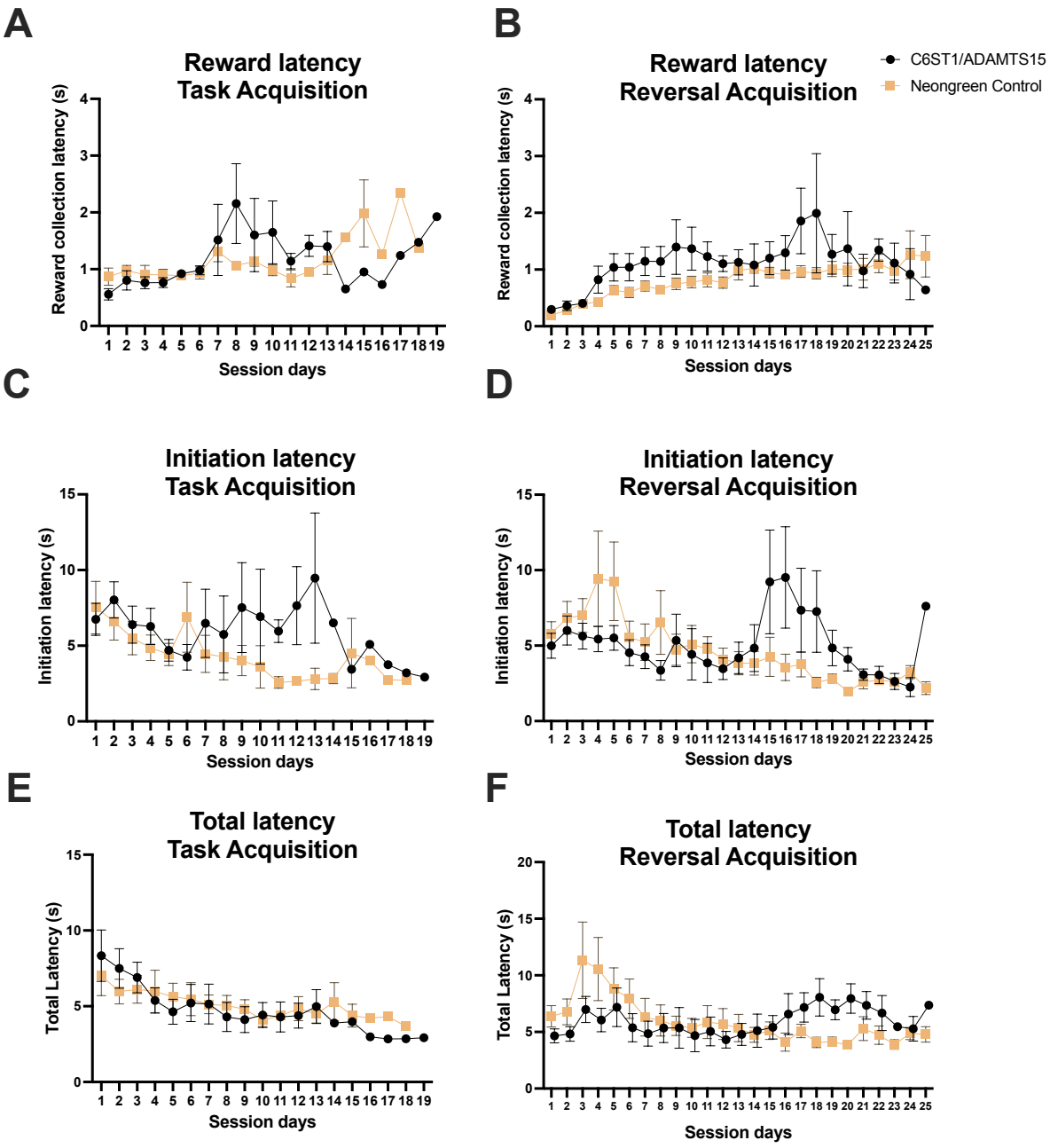

Figure 18. Latencies for reward collection, trial initiation and total latency across session days. The plot displays latencies over session days for both the experimental (n=9) and control group (n=7). The plot presents mean ± SEM. **A-B)** Reward collection latency for task and reversal acquisition, respectively. **C-D)** Initiation latency for task and reversal acquisition **E-F)** Total latency for task and reversal acquisition.

3.2.6 The experimental group has more screen touches during intertrial intervals and more beam breaks

The amount of screen touches during the intertrial interval and total beam breaks can be used to indicate activity. During task acquisition, more screen touches during the intertrial interval were observed for the experimental group (unpaired parametric t-test, $t(14) = 3.706$, p-value = 0.0023). Individual variation in screen touches was observed for the experimental group compared to the controls (Figure 19A) during task acquisition, while the spread was more similar between the groups in the reversal acquisition (Figure 19B). The experimental group had slightly more touches in reversal, but this difference was insignificant (Mann-Whitney U, p-value = 0.2991). For total beam breaks, the movement in the chamber, a similar trend was seen with the experimental group having significantly more beam breaks than the controls (unpaired parametric t-test, $t(14) = 3.261$, p-value =0.0057) (Figure 19C). In the reversal acquisition, the experimental group had slightly more beam breaks, but there was no significant difference (unpaired parametric t-test, $t(14) = 1.078$, p-value =0.2993).

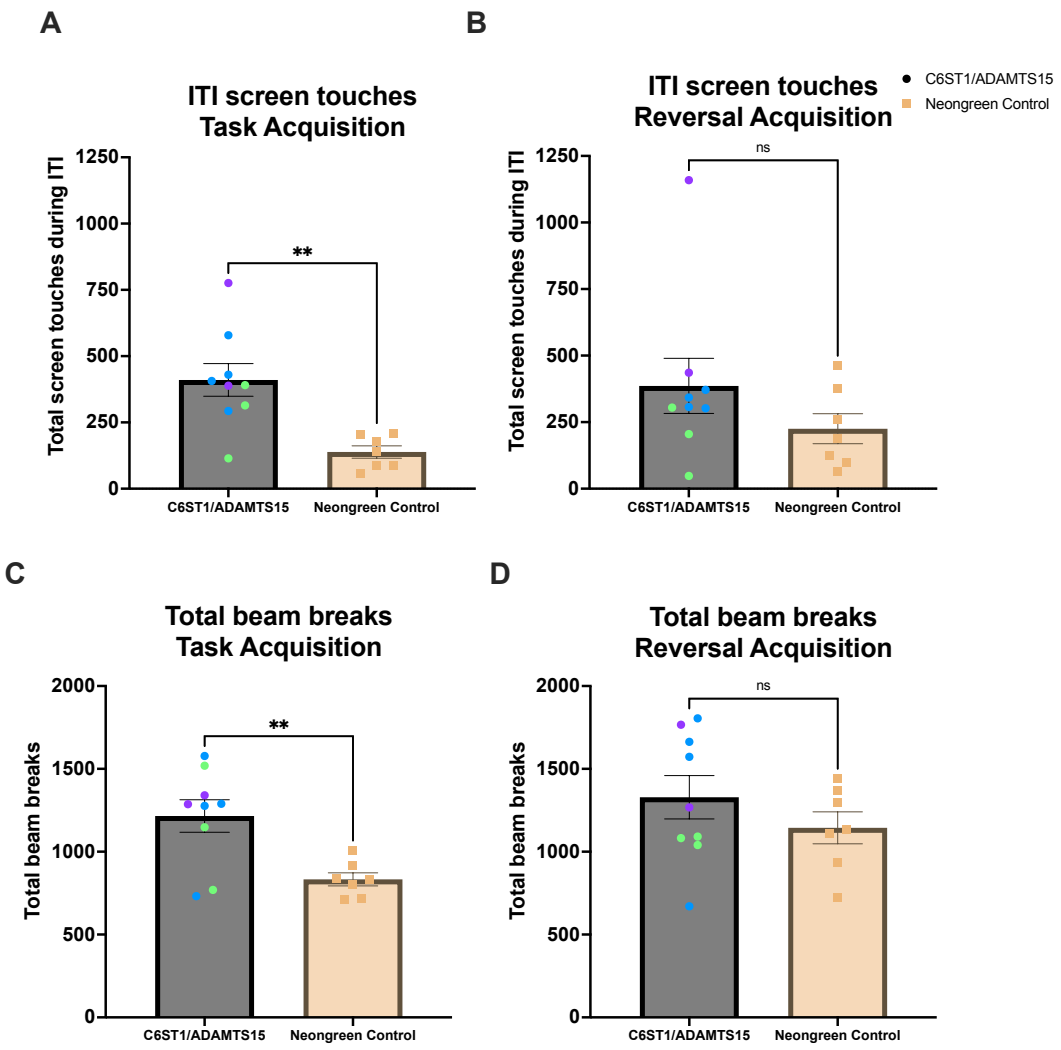

Figure 19. Total screen touches during the ITI and total beam breaks. Each dot represents the average values of individual mice for the experimental (n=9) and control group (n=7). Blue dots indicate a bilateral injection of PL and IL, green dots for unilateral + IL on the other hemisphere (mix), and purple for unilateral. The dotted line represents the cut off day for each task. The bar plots present the mean ± SEM for both groups. **A)** Total screen touches during ITI for task acquisition, measured by unpaired parametric t-test, p-value = 0.0023, p <0.5 is indicated by *. **B)** Total screen touches during ITI for reversal acquisition, measured by Mann-Whitney U, p-value = 0.2991. **C)** Total beam breaks for task acquisition, measured by unpaired parametric t-test, p-value = 0.0057. **D)** Total beam breaks for reversal acquisition, measured by unpaired parametric t-test, p-value = 0.2993.

4. Discussion

In this study, we used a new method to examine for PNN perturbations. Viral vectors were applied to overexpress C6ST1 in combination with CRISPR activation of ADAMTS15 to modulate the PNNs in the mPFC. This resulted in reduced WFA staining in the areas of the viral injections. There was a slight reduction with C6ST1, and no reduction with ADAMTS15 alone or for the controls. This indicated an important role of both constructs combined in the modulation of the PNNs. This reduction suggests that the activity of the metalloproteinase ADAMTS15 is dependent on an increase in C6S sulphation to digest the PNNs. An effect of the PNN modulation was seen in the behavioural task, in which the experimental animals spent more time during the sessions in task acquisition, needed fewer days to complete reversal acquisition, and were generally more active. These effects seem to be more profound in the bilateral subgroup, which might suggest that the amount of viral injection might be important. However, due to the injections' spread, any PNN perturbation functions cannot be confined to the mPFC.

4.1 PNN perturbations with viral delivery compared to previous methods

In the current study, we introduced a new method of PNN perturbations by using a combination of overexpression and CRISPRa delivered with AAVs. A study by (Rossier et al., 2015) found that ADAMTS15 was preferentially expressed in fast-spiking PV cells with PNNs, indicating its activity might be PNN-specific. However, as the mRNA expression increases only during certain events in development, it might be specifically active to maintain the heightened plasticity early in life. This could mean that using CRISPRa to express this gene from the endogenous loci, may be a more specific method of targeting the PNNs than using exogenous enzymes (Heidersbach et al., 2023). The use of AAV may also exhibit a more stable gene expression over longer periods of time compared to the attenuating effect of the ChABC treatments, as several injections are usually needed for longer experiments (Lin et al., 2007). This method opens the possibility of altering the PNNs more naturally by utilising mechanisms that may happen in the cells during development. As the mechanisms behind the PNN modulation are unknown, this will only be speculations at best, and further testing is needed for any conclusions. Previous ways of studying the PNNs have included digestion of the CSPG with the enzyme ChABC, i*n vitro* models, viral injections and knockout models. *In vitro* studies of PNNs have given valuable insight of PNN components and

their role in PNN formation but might not represent the PNN's role *in vivo* (Giamanco et al., 2010; Kwok et al., 2010). Mechanisms in an organism are more complex than *in vitro* experiments, as these are usually isolated or may only represent certain environments. For example, examining the aggrecan's role in PNN formation has mostly been performed *in vitro*, as *in vivo* studies have been challenging due to the importance of aggrecan in cartilage. Mutations in the gene encoding it, ACAN, cause embryonic lethality (Rittenhouse et al., 1978).

For *in vivo* experiments, knock-out models can be helpful. Knocking out genes encoding PNN components can further our knowledge of how these components work and their contribution to the PNNs. These studies have been valuable in studying the formation and development of the PNNs, as certain knockouts have been shown to disrupt its formation (Carulli et al., 2010; Rowlands et al., 2018). However, global knockouts of certain components might not represent the normal functions of the PNNs as their composition differs, and the components themselves are implicated in other functions. ChABC has also been widely used in PNN research to digest CSPGs (Fawcett et al., 2019). However, this enzymatic treatment is not specific to the PNNs and digest CSPGs indifferent to their sulphation and digest CSPGs in the surrounding areas. Other aspects of this treatment that need to be considered are how long the enzyme is active, the variability in concentrations between labs and the timing of injections. Although more testing is necessary, the method in this study provides a new means of exploring PNN perturbations and their functions in a more specific way. It is important to notice that this method may be more specific by using an endogenous enzyme and sulfotransferase. However, it is still not entirely PNN specific, as C6ST1 and ADAMTS15 will be expressed by all cells infected.

4.2 Extensive spread of viral injection

Visual inspection of the histological results and the alignment of customised atlases displayed an extensive spread of the virus. This was caused by large injection volumes of 300 nl injected in each depth in both hemispheres. The amount was chosen to increase the possibility of hitting the target locations and elicit a large response of the PNN perturbations. This resulted in a viral injection that hit the target locations but the injection was not confined to the mPFC targeted through PL and IL (Figure 10Ai-iii+Bi-iii). The gene expression was observed in several other brain areas (Appendix A, Supplementary Table 2). Although the spread was variable for the different

animals, the virus injections usually spread along the midline of the brain. Brain sections for immunohistochemistry analyses were only collected at a certain distance from and around the target coordinates, which may limit the opportunity to inspect the full anterior and posterior spread in the brain. The spread could, therefore, be more extensive than reported here. The posterior brain sections in Figure 10Aiii+Biii also indicated that the viral injection might have leaked into the ventricles, meaning the spread could be even greater. Another important aspect is that the ADAMTS15 injection was not detectable due to insufficient antibody labelling and could not be visualised. Replicating the experiments with optimised injection volumes could help limit any confounding effects of gene expression in other brain areas and better our understanding of PNN modulation in the mPFC through the behavioural task.

4.3 Reduced WFA staining from the combination of C6ST1 and ADAMTS15

From visual inspection of the histological results, reduced intensity in the WFA staining was observed after treatment with the viral constructs giving a combined expression of C6ST1 and ADAMTS15 (Figure 11Ai+iii). This reduction was not observed in the controls (Figure 11Bi-iii) or for the CRISPRa of ADAMTS15 (Figure 11Ci-iii). As no reduction in WFA intensity was seen for the injection of the ADAMTS15 construct, it suggests that the ADAMTS15 might not cleave components in the PNNs on its own. This could result from no expression, too low concentration of ADAMTS15, or the ADAMTS15 might need a particular environment to regulate its activity. By mimicking the increased levels of C6S found during development with the overexpression of the C6ST1 it could increase the activity of the ADAMTS15. A study found that the ADAMTS5, another type of ADAMTS, was found to cleave aggrecan more efficiently with increased levels of C6S (Miyata & Kitagawa, 2016). This suggests that the C6S levels can affect the levels of aggrecan. If aggrecan levels are low during the critical period, this could also affect the formation of the PNNs. A study using an aggrecan knockout mouse line, found no WFA positive PNNs in the adult brain (Rowlands et al., 2018). This suggests that aggrecan is necessary for PNN formation. If the proteinase activity is upregulated during the critical periods, where C6S levels are high and heightened plasticity is needed, it can indicate that the proteases are needed to avoid the formation of PNNs by cleaving their components. As the C6S slowly decreases, it might decrease the activity of the proteases, resulting in more aggrecan and formation of the PNNs. The reduced intensity in the WFA staining after treatment therefore supports our hypothesis that the PNNs

are digested. This may induce a juvenile-like state of plasticity similar of that during the critical periods (Lensjø, Lepperød, et al., 2017). This suggests that the ADAMTS15 might be important for developmental regulation of the PNNs and are important for controlling the plasticity of the critical periods.

A slight decrease in the intensity of the WFA staining was seen for the C6ST1 viral construct injection (Figure 11Di-iii). It is, however, important to note that the mice with the separate injections were only housed for four weeks after the surgeries to allow for viral expression. The mice that conducted the visual discrimination task were housed for longer (+/- two months) and thus exposed to longer viral expression. This poses the question of whether the effect of the C6ST1 on the WFA staining would be equal to the combination if exposed to the same degree of viral gene expression. The small reduction in the WFA staining of the mouse with only the C6ST1 construct could, therefore, indicate that the C6S alone can influence the PNN structure (Figure 11Dii+iii). A study by Miyata et al., (2012) found that transgenic mice overexpressing C6ST1 showed a reduction in the WFA staining during and after the critical period compared to controls. In the transgenic mice, they also found an increase of PNN-like structures recognised by a C6S antibody and that these seldomly colocalised with the WFA staining (Miyata et al., 2012). These C6S-enriched structures were not observed in the wild-type animals. This suggests that the C6S might be important for the conventional WFA positive formation of the PNNs (Miyata et al., 2012). Immunostaining of C6S was performed in the current study to see whether the C6ST1 (whose presence was validated from the mScarlet) did catalyse C6S. Staining of the C6S was observed in the animals with injections containing the C6ST1 construct (Figure 13Aii-iii + 13Dii-iii) and not in the controls (Figure 13Bii-iii) or in the ADAMTS15 alone (Figure 13Cii-ii). Indeed, this indicates that the C6S was catalysed by the C6ST1.

As a slight reduction in the intensity of WFA was observed for the mouse with the C6ST1-only construct, it suggests that the sulphation patterns might have changed the binding properties of WFA. The WFA is thought to bind the N-acetyl-D-galactosamine of the CS-GAG chains (Härtig et al., 2022). To visualise if the PNNs were still present, aggrecan staining was performed, as the aggrecan antibodies have been shown to overlap with WFA staining but also stain different types

of PNNs (Matthews et al., 2002; Rowlands et al., 2018). The aggrecan antibody did not stain any PNNs in the mPFC but did stain a few PNNs in other areas around the substansia inomiata/nucleus accumbens (Figure 12Ai). As neither the WFA nor aggrecan staining was observed around the viral combination injection, it suggests that the PNNs are absent. The aggrecan in the PNNs may therefore have been cleaved by ADAMTS15, resulting in the removal of the PNNs. This could, however, be a result of a non-optimal aggrecan staining. As quantification was not performed in this study and the validation of the ADAMTS15 was not observed, further testing is needed. To validate the presence of ADAMTS15, new antibody staining should be conducted, or its mRNA expression can be validated through quantitative polymerase chain reaction. This was not performed in the current study due to limited time. Quantification of the WFA, a larger dataset of mice and further staining of the PNN components would be needed for conclusive results. Although more testing is needed to better understand the mechanisms behind this modulation, the results are promising and indicate that modulation of the PNN has occurred.

4.4 The effect of PNN perturbation on learning in a visual discrimination task

A visual discrimination task with reversal was performed in a touchscreen operant chamber to assess whether the PNN perturbation in the mPFC affects learning. The number of days needed to reach the criterion can suggest how fast the new stimulus-reward association have been learned. The current study found that all mice acquired the visual discrimination task within 25 days (Figure 14A). When divided into subgroups, each group spent a similar number of days to reach the criterion, with an exemption of the unilateral group, which displayed a higher mean. This is most likely due to the low performance of one of the animals, and with a group size of only two, a large effect will be seen. In combination, the experimental group spent, on average, 12 days, while the controls spent 10 days (Figure 15A). These results were similar to that of other studies using the same strain, ranging from acquiring the task within an average of 8-12 days (Horner et al., 2013; Piiponniemi et al., 2017). As the experimental and control groups used a similar number of days, no difference was detected, suggesting that the PNN perturbation might not affect the initial stage of learning. These results were unexpected, as we thought the PNN perturbations would increase plasticity, resulting in faster learning. While the PNN perturbations did not seem to affect the initial learning of the task, an effect was seen in the reversal stage. Similar effects were again seen for the bilateral and mix subgroups (Figure 14B), while the

unilateral spent similar number of days as the controls. Although only two animals, this might indicate that a bilateral injection is needed for more profound effects of the PNN perturbations. The experimental group used fewer days to complete the reversal, while many controls did not meet the criterion (Figure 15B). This suggests that the controls struggled to adapt to the reversed visual cue more than the experimental group. As the mPFC has been implicated in cognitive flexibility and adaptive goal directed responding (Hamel et al., 2022; Jett et al., 2017), the perturbations could have influenced the ability to flexibly change the previously learnt reward association but did not affect the initial learning of the task. A potential reason for this could be that the rewiring of the circuits was easier without the presence of the PNNs or in the presence of increased C6S. A study of ECM removal in the auditory cortex of Mongolian gerbils found an improved reversal task performance but no effect on the learning acquisition in an auditory discrimination task (Happel et al., 2014). This effect on the reversal was only seen when the ECM was removed between the two tasks and not by ECM removal before the initial learning phase. Animals with ECM removal before the initial learning task performed similarly to the saline-treated animals, which either failed or struggled to discriminate between the stimulus frequencies in the reversal task. This removal was performed by injecting an enzyme, hyaluronidase, which cleaves hyaluronic acid, the backbone of PNNs. However, they observed that the ECM reconstitution started nine days after injections, close to the start of the reversal, which may be a reason for the little effect seen in the reversal. A proposed reason why this was not observed in our study could be that the effect of the long-lasting viral expression may be more profound in reversal, compared to their injection which reconstituted after day 9. The additional effect of the C6S could also be a reason for the difference.

The performance curve displays the percent correct choices and suggests the animal's accuracy in discriminating between the correct and incorrect stimuli, indicating an understanding of the task. Similarities in the performance rate was seen for the different subgroups and controls (Figure 14C). For the combined groups, a slight difference in correct choices was observed for the first day of task acquisition, in which the controls performed slightly better (Figure 16A). This could result from pure chance or indicate a slight stimulus bias (Horner et al., 2013) as the initial performance was expected to be around chance level due to random responses. The experimental group's performance was around chance level for the first four days, while this was

not seen for the control group. Although the controls started with slightly better performance, the slope of their performance was less steep than that of the experimental group after day 4. This sudden increase in performance for the experimental group might indicate that once the association between the stimulus and reward was understood, they learned the task in a fast manner. As the performance curves for both groups steadily increased, it suggested that both groups gradually became better at visually discriminating between the correct and incorrect stimuli. For reversal, the different subgroups displayed similar trends, both bilateral and mix had slightly steeper performance slopes compared to controls and unilateral (Figure 14D). The combined groups in reversal started around 20 percent, which was expected due to the reversal of the visual cues. A steady increase was seen for both groups, indicating that they gradually adapted to the new correct stimulus. From visual inspection of Figure 16B the experimental group had a slightly steeper increase in reversal compared to the controls, which could support their ability of adaptation. However, as both groups displayed relatively similar performance curves for both task and reversal, it is likely that the PNN perturbation does not affect the accuracy of a visual discrimination task. In this current study, no analyses were based on the slopes of the curves, and differences were therefore assessed based on visual inspections. Further analyses, and larger samples sizes could give us more knowledge about the PNN perturbations effect on accuracy.

Additional parameters were inspected to assess the effect of the PNN perturbations. The experimental group spent on average longer time during the sessions (Figure 17A) and in the first sessions of task acquisition, based on visual inspection of the plot (Figure 17B). The time plots display the opposite trends of the performance curves, as the time spent seems dependent on the animal's performance. Several factors may influence this: the number of trials completed, the number of incorrect responses (correction trials + delays), motivation (initiation latency and reward collection), decision time and the overall activity of the animal. The experimental group spent similar time in collecting rewards (Figure 18A) and for decisions (Figure 18E) as the controls but did spend slightly more time in initiating the trials mid-task based on visual inspections of Figure 18C. This indicates that both groups were motivated for the task and that the vanilla soymilk was efficient as a positive reinforcement. Motivational deficits can result from differences in body weight, as the food restriction drives the motivation towards the reinforcement. Although

some variations were seen in the current study, the body weights of the animals were in similar ranges (Appendix C, Supplementary Figure 1). A higher number of screen touches (Figure 19A) and beam breaks (Figure 19C) were also observed for the experimental group than the controls, indicating higher activity. This higher activity could be a result of lower anxiety. A recent study by Grødem et al. (unpublished) did show that mice with a knockout of aggrecan in the PV cells, and therefore lacking PNNs, showed a lower anxiety-like behaviour in the Morris water maze and open field test. Although PNN removal in our study is not restricted to the PV cells, this might indicate that the PNN perturbations might affect behaviour in terms of anxiety. It could, therefore, be interesting to test this new perturbation in an open field or Morris water maze to compare the behaviour.

On average, both groups spent similar time during sessions (Figure 17C). As performance progress was more similar in reversal, this was also reflected in the time spent (Figure 17D). Some variation was seen in both reward collection (Figure 18B) and initiation latency (Figure 18D) but were generally similar. The controls spent slightly longer deciding on the stimulus at the start of the reversal (Figure 18F), which could indicate that they struggled a bit more to decide when the cues were reversed. The experimental group's screen touches (Figure 19B) and total beam breaks (Figure 19D) were slightly higher but closer to the controls than in task acquisition. More variability in different parameters was seen during task acquisition compared to reversal for the experimental group. One could suggest that introducing a new task will cause more variability than reversal, as the task principles are already learned when starting the reversal.

4.5 Methodological considerations

The design of this study gave rise to some challenges in which many variables were tested at once. A combination of two viral constructs was used to assess their conjunctive functions in PNN regulation in the same animals. Although this took the three R's into consideration, it made it difficult to say whether the effects were based on the combination or their separate function. Further testing of the separate constructs, with or without the behavioural task, would have been interesting. The large volume of the viral injections was used to elicit a response, but the extensive spread made it difficult to conclude any function of the PNN perturbations in the mPFC. The behavioural effects could result from the combined brain areas infected, and a smaller injection volume would be important to assess the effects in specific regions. As the antibodies for ADAMTS15 did not work, it was impossible to conclude that the ADAMTS15 was expressed, although the differences in WFA staining suggested so.

4.5.1 Coordinates and microinjections

Coordinates are crucial for targeting the correct brain areas and are often based off reference atlases (Franklin & Paxinos, 2007). As the reference atlas is based on a particular strain of mice, it is important to notice that variability between strains, animals, age and sex can cause deviations from the original coordinates (Spring et al., 2007). As most coordinates are based on the stereotaxic locations of bregma and lambda (Figure 7A), variations in the skull sutures may also lead to incorrect coordinates. The coordinates are, therefore, dependent on the measurements of the surgeon during stereotaxic surgeries. Testing and optimising the coordinates should always be performed before the experiments start. In this study, the coordinates from The Mouse Brain Atlas (Franklin & Paxinos, 2007) had to be adjusted to fit my measurements better.

Stereotaxic surgeries were performed for the microinjections and is a procedure which requires skills and precision. It harbours many challenges, as minor errors will affect the targeting of brain structures. Head levelling of the animal is a complex procedure which requires practice and experience. Adjustments must be made for each animal, and minor errors in the angles can lead to inaccurate targeting. Another source of error is the craniotomy. As the coordinates used in this study were close to a sinus, small craniotomies were used to avoid puncturing the sinus. The small

craniotomies made it difficult to assess the brain surface, which could have resulted in deeper injections than preferred. The exact location was, however, difficult to assess due to the large injection volumes. For injections, thin glass pipettes were pulled from glass capillaries. Thinner glass pipettes are vulnerable to clogging but cause less tissue damage, while a thicker pipette has the opposite properties and can cause leakage. For the two animals in the unilateral subgroup, clogging of the pipette was most likely the reason for the lack of injection in the other hemisphere.

The volume of the microinjection surgeries is equally important. Spread of virus injections will most likely occur with any injections but can be limited by optimising the injection volume. While a lower injection volume can limit spread, a higher precision will be needed to hit the same location for each injection, which is important for comparing the results. In the current study, a larger volume was chosen to increase the probability of hitting the same area in each animal. However, this came at the cost of assessing any effects of specific brain areas on the behavioural results. Further optimisation of the injections and volume should be performed to increase precision and to limit the spread of the virus.

4.5.2 Immunohistochemistry and imaging

All brain sections were stained using the approach of free-floating sections because it allows for better penetration of antibodies compared to other methods, such as staining of already mounted sections. However, this approach includes transferring brain sections between the wells for all stages of immunostaining, which increases the chance of section tearing and section-section adhering, a problem I encountered in the current study. A small amount of sections per well and well strainers could prevent these issues, but comes at the cost of antibody volumes needed. As many of the antibodies tested in the current study did not work, an effort should be placed to test new antibodies. Different combinations of staining that would be of interest could be PV, WFA and C6S to test the specificity of the injections to PV cells and to see the localisation of WFA and C6S. Additional positive and negative controls for the ADAMTS15 in mPFC at different developmental stages would be interesting to further our knowledge of its expression and improve the interpretation of the histological results.

4.5.3 Cryosectioning and atlases

One of the major challenges when using a cryostat is slicing the sections at the perfect angle. As angles in the brain sections give uneven presentations of the two hemispheres, it is hard to assess locations and identify the borders of brain areas. Uneven brain sections were one of the challenges faced in the current study, which made it difficult to assess the scope of the injections according to the position from bregma and regarding the atlas customisation. As angles can be difficult to assess from visual inspection, Quint workflow was used. This tool allows for a more accurate assessment of atlases to brain sections as angles and spacing are considered in the QUICKNII software (Yates et al., 2019). Although it helped with the spacing and alignment, the uneven sectioning still resulted in morphed atlases, making it difficult to assess the brain area borders. Therefore, the atlases created in this study should only be used as guidance. Downstream features of the Quint workflow also allow for the quantification of labelled cells and can give a more accurate representation of the injections (Yates et al., 2019).

4.5.4 Touchscreen operant chamber

Touchscreen operant chambers were conducted for the visual discrimination task in the current study. The touchscreen platform is a great tool for behavioural testing of rodents and is advantageous in many ways. It allows for simultaneous testing of many animals, low experimenter involvement, more objective assessment of behaviour, and various parameters to analyse (Horner et al., 2013). The low level of experimental involvement and the standardisation of the platform can increase the experimental replication between labs. As this is an appetitive behavioural testing method, food restriction is needed. In the current study, we housed a mix of control and experimental mice in each cage, with around three to four mice in each cage. For their well-being, housing them together is best, but it makes it difficult to obtain the same percentage body weight for each mouse, as competition for food does occur. To solve this problem, the mice could be housed separately, or water restrictions could be implemented. It is, however, important to think about the well-being of the animals and that water restriction may affect their performance in different ways than food restriction does (Goltstein et al., 2018).

4.6 Future perspectives

The work presented in the current study is a great starting point for developing methods for specific targeting of the PNNs. However, due to inconclusive results, further testing or a replication of the study would be needed. Quantifying the histological results should be performed to validate the effect of the PNN perturbations, and qPCR could be performed to validate the expression of the ADAMTS15. Assessment of the two constructs would also be necessary to ensure that the combination is needed for the PNN perturbation and that it is not an effect of the C6S on the WFA staining. Optimising the staining of the PNNs could be done by staining a mixture of WFA and anti-aggrecan antibodies with the same colour to reveal a wider range of PNNs (Härtig et al., 2022). To make this method more precise, transgenic mice can be used for PV-dependent cre expression, as seen by Oh et al., (2017). This method uses the cre/loxP system, where gene expression can be targeted to specific cell types. PNNs could, therefore, be targeted through PV-specific transgene expression.

A comparison should be made between this method, and other common methods, such as ChABC digestion. This could give valuable information on the difference between utilising the cell's enzymes to perturb the PNNs and the effect of introducing a bacterial enzyme. Comparisons should be assessed using histological methods at different time points to compare the effects of the treatments. Electrophysiological recordings could also be of interest to assess how the perturbations affect the plasticity and activity of neurons.

To strengthen the results of the behavioural results and statistics, increasing the sample size would be needed. As a difference was seen according to the injection success, it would be interesting to replicate the experiments with more individuals in unilateral and bilateral to assess the effect of different amounts of viral expression. An optimisation of the injection volumes and coordinate testing could also be of interest to assess the effects of PNN perturbations on specific brain areas. Additional histological testing at different time intervals for both untrained and trained animals could be useful to detect any differences in the brain at different stages of learning compared to untrained animals.

5. Conclusion

The histological results, indicated that the new method tested, did cause PNN perturbations. Based on the preliminary results, WFA staining intensity was reduced in the locations of the viral injections overexpressing C6ST1 and CRISPR-activating the expression of ADAMTS15. The overexpression of C6ST1 was validated through the fluorescent protein mScarlet, and the catalysation of the C6 sulphation was observed by antibody staining. Efforts were made to validate the expression of ADAMTS15 but were not obtained due to insufficient antibody staining. However, the reduced WFA staining was only observed for the combination, indicating the ADAMTS15s presence. These results imply that combined overexpression of C6S and ADAMTS15 can perturb the PNNs. Although further testing is needed, these results can open a new field of PNN research.

Results from the visual discrimination task suggest that the PNN perturbations did not affect the initial learning of the visual discrimination task but significantly affected learning once the visual cues were reversed. Animals with PNN perturbations spent fewer days completing reversal acquisition and seemed more susceptible to adapting the new correct stimulus than the controls. Indicating that the PNN perturbations in the mPFC might affect the cognitive flexibility needed for reversal acquisition. However, due to the spread of the viral injections, the effect of the PNN perturbations cannot be contained to the functions of the mPFC.

6. References

Abela, A. R., & Chudasama, Y. (2013). Dissociable contributions of the ventral hippocampus and orbitofrontal cortex to decision-making with a delayed or uncertain outcome. *European Journal of Neuroscience*, *37*(4), 640–647. https://doi.org/10.1111/ejn.12071

Anastasiades, P. G., & Carter, A. G. (2021). Circuit organization of the rodent medial prefrontal cortex. *Trends in Neurosciences*, *44*(7), 550–563. https://doi.org/10.1016/j.tins.2021.03.006

Anderson, M. D., Paylor, J. W., Scott, G. A., Greba, Q., Winship, I. R., & Howland, J. G. (2020). ChABC infusions into medial prefrontal cortex, but not posterior parietal cortex, improve the performance of rats tested on a novel, challenging delay in the touchscreen TUNL task. *Learning & Memory*, *27*(6), 222–235. https://doi.org/10.1101/lm.050245.119

Arain, M., Sharma, S., Mathur, Rais, Nel, Sandhu, Haque, & Johal. (2013). Maturation of the adolescent brain. *Neuropsychiatric Disease and Treatment*, 449. https://doi.org/10.2147/NDT.S39776

Bear, M. F., Connors, B. W., & Paradiso, M. A. (2001). *Neuroscience: Exploring the brain* (2nd ed). Lippincott Williams & Wilkins.

Berardi, N., Pizzorusso, T., & Maffei, L. (2000). Critical periods during sensory development. *Current Opinion in Neurobiology*, *10*(1), 138–145. https://doi.org/10.1016/S0959-4388(99)00047-1

Bliss, T. V. P., & Collingridge, G. L. (1993). A synaptic model of memory: Long-term potentiation in the hippocampus. *Nature*, *361*(6407), 31–39. https://doi.org/10.1038/361031a0

Brocker, C. N., Vasiliou, V., & Nebert, D. W. (2009). Evolutionary divergence and functions of the ADAM and ADAMTS gene families. *Human Genomics*, *4*(1), 43. https://doi.org/10.1186/1479-7364-4-1-43

Brückner, G., Hausen, D., Härtig, W., Drlicek, M., Arendt, T., & Brauer, K. (1999). Cortical areas abundant in extracellular matrix chondroitin sulphate proteoglycans are less affected by cytoskeletal changes in Alzheimer's disease. *Neuroscience*, *92*(3), 791–805. https://doi.org/10.1016/S0306-4522(99)00071-8

Burnside, E. R., & Bradbury, E. J. (2014). Review: Manipulating the extracellular matrix and its role in brain and spinal cord plasticity and repair: Manipulating the matrix for CNS repair. *Neuropathology and Applied Neurobiology*, *40*(1), 26–59. https://doi.org/10.1111/nan.12114

Carlén, M. (2017). What constitutes the prefrontal cortex? *Science*, *358*(6362), 478–482. https://doi.org/10.1126/science.aan8868

Carulli, D., Pizzorusso, T., Kwok, J. C. F., Putignano, E., Poli, A., Forostyak, S., Andrews, M. R., Deepa, S. S., Glant, T. T., & Fawcett, J. W. (2010). Animals lacking link protein have attenuated perineuronal nets and persistent plasticity. *Brain*, *133*(8), 2331–2347. https://doi.org/10.1093/brain/awq145

Challis, R. C., Ravindra Kumar, S., Chan, K. Y., Challis, C., Beadle, K., Jang, M. J., Kim, H. M., Rajendran, P. S., Tompkins, J. D., Shivkumar, K., Deverman, B. E., & Gradinaru, V. (2019). Systemic AAV vectors for widespread and targeted gene delivery in rodents. *Nature Protocols*, *14*(2), 379–414. https://doi.org/10.1038/s41596-018-0097-3

Chudasama, Y., & Robbins, T. W. (2003). Dissociable Contributions of the Orbitofrontal and Infralimbic Cortex to Pavlovian Autoshaping and Discrimination Reversal Learning: Further Evidence for the Functional Heterogeneity of the Rodent Frontal Cortex. *The Journal of Neuroscience*, *23*(25), 8771–8780. https://doi.org/10.1523/JNEUROSCI.23-25-08771.2003

Cook, R. G., Geller, A. I., Zhang, G.-R., & Gowda, R. (2004). Touchscreen-enhanced visual learning in rats. *Behavior Research Methods, Instruments, & Computers*, *36*(1), 101–106. https://doi.org/10.3758/BF03195555

Deepa, S. S., Carulli, D., Galtrey, C., Rhodes, K., Fukuda, J., Mikami, T., Sugahara, K., & Fawcett, J. W. (2006). Composition of Perineuronal Net Extracellular Matrix in Rat Brain. *Journal of Biological Chemistry*, *281*(26), 17789–17800. https://doi.org/10.1074/jbc.M600544200

Deepa, S. S., Umehara, Y., Higashiyama, S., Itoh, N., & Sugahara, K. (2002). Specific Molecular Interactions of Oversulfated Chondroitin Sulfate E with Various Heparin-binding Growth Factors. *Journal of Biological Chemistry*, *277*(46), 43707–43716. https://doi.org/10.1074/jbc.M207105200

Ding, X., Yu, L., Chen, L., Li, Y., Zhang, J., Sheng, H., Ren, Z., Li, Y., Yu, X., Jin, S., & Cao, J. (2022). Recent Progress and Future Prospect of CRISPR/Cas-Derived Transcription Activation (CRISPRa) System in Plants. *Cells*, *11*(19), 3045. https://doi.org/10.3390/cells11193045

Domingues, K., Melleu, F. F., & Lino De Oliveira, C. (2021). *Medial Prefrontal Cortex controlling the immobility of rats in the forced swimming test: A systematic review and meta-analysis* [Preprint]. Animal Behavior and Cognition. https://doi.org/10.1101/2021.04.27.441685

Erisir, A., Lau, D., Rudy, B., & Leonard, C. S. (1999). Function of Specific K^+ Channels in Sustained High-Frequency Firing of Fast-Spiking Neocortical Interneurons. *Journal of Neurophysiology*, *82*(5), 2476–2489. https://doi.org/10.1152/jn.1999.82.5.2476

Favuzzi, E., Marques-Smith, A., Deogracias, R., Winterflood, C. M., Sánchez-Aguilera, A., Mantoan, L., Maeso, P., Fernandes, C., Ewers, H., & Rico, B. (2017). Activity-Dependent Gating of Parvalbumin Interneuron Function by the Perineuronal Net Protein Brevican. *Neuron*, *95*(3), 639-655.e10. https://doi.org/10.1016/j.neuron.2017.06.028

Fawcett, J. W., Oohashi, T., & Pizzorusso, T. (2019). The roles of perineuronal nets and the perinodal extracellular matrix in neuronal function. *Nature Reviews Neuroscience*, *20*(8), 451–465. https://doi.org/10.1038/s41583-019-0196-3

Franklin, K. B. J., & Paxinos, G. (2007). *The mouse brain in stereotaxic coordinates* (3. ed). Elsevier, AP.

Giamanco, K. A., Morawski, M., & Matthews, R. T. (2010). Perineuronal net formation and structure in aggrecan knockout mice. *Neuroscience*, *170*(4), 1314–1327. https://doi.org/10.1016/j.neuroscience.2010.08.032

Golgi, C. (1898). *Intorno alla struttura delle cellule nevose*. Bolet. Soc. Med.-Chir. Pavia 1.

Goltstein, P. M., Reinert, S., Glas, A., Bonhoeffer, T., & Hübener, M. (2018). Food and water restriction lead to differential learning behaviors in a head-fixed two-choice visual discrimination task for mice. *PLOS ONE*, *13*(9), e0204066. https://doi.org/10.1371/journal.pone.0204066

Hamel, L., Cavdaroglu, B., Yeates, D., Nguyen, D., Riaz, S., Patterson, D., Khan, N., Kirolos, N., Roper, K., Ha, Q. A., & Ito, R. (2022). Cortico-Striatal Control over Adaptive Goal-Directed Responding

Elicited by Cues Signaling Sucrose Reward or Punishment. *The Journal of Neuroscience*, *42*(18), 3811–3822. https://doi.org/10.1523/JNEUROSCI.2175-21.2022

Happel, M. F. K., Niekisch, H., Castiblanco Rivera, L. L., Ohl, F. W., Deliano, M., & Frischknecht, R. (2014). Enhanced cognitive flexibility in reversal learning induced by removal of the extracellular matrix in auditory cortex. *Proceedings of the National Academy of Sciences*, *111*(7), 2800–2805. https://doi.org/10.1073/pnas.1310272111

Härtig, W., Meinicke, A., Michalski, D., Schob, S., & Jäger, C. (2022). Update on Perineuronal Net Staining With Wisteria floribunda Agglutinin (WFA). *Frontiers in Integrative Neuroscience*, *16*, 851988. https://doi.org/10.3389/fnint.2022.851988

Hebb, D. O. (1949). *The Organization of Behavior* (0 ed.). Psychology Press. https://doi.org/10.4324/9781410612403

Heidersbach, A. J., Dorighi, K. M., Gomez, J. A., Jacobi, A. M., & Haley, B. (2023). A versatile, high-efficiency platform for CRISPR-based gene activation. *Nature Communications*, *14*(1), 902. https://doi.org/10.1038/s41467-023-36452-w

Horner, A. E., Heath, C. J., Hvoslef-Eide, M., Kent, B. A., Kim, C. H., Nilsson, S. R. O., Alsiö, J., Oomen, C. A., Holmes, A., Saksida, L. M., & Bussey, T. J. (2013). The touchscreen operant platform for testing learning and memory in rats and mice. *Nature Protocols*, *8*(10), 1961–1984. https://doi.org/10.1038/nprot.2013.122

Hylin, M. J., Orsi, S. A., Moore, A. N., & Dash, P. K. (2013). Disruption of the perineuronal net in the hippocampus or medial prefrontal cortex impairs fear conditioning. *Learning & Memory*, *20*(5), 267–273. https://doi.org/10.1101/lm.030197.112

Jakovljević, A., Tucić, M., Blažiková, M., Korenić, A., Missirlis, Y., Stamenković, V., & Andjus, P. (2021). Structural and Functional Modulation of Perineuronal Nets: In Search of Important Players with Highlight on Tenascins. *Cells*, *10*(6), 1345. https://doi.org/10.3390/cells10061345

Jett, J. D., Bulin, S. E., Hatherall, L. C., McCartney, C. M., & Morilak, D. A. (2017). Deficits in cognitive flexibility induced by chronic unpredictable stress are associated with impaired glutamate

neurotransmission in the rat medial prefrontal cortex. *Neuroscience*, *346*, 284–297. https://doi.org/10.1016/j.neuroscience.2017.01.017

Jinek, M., Chylinski, K., Fonfara, I., Hauer, M., Doudna, J. A., & Charpentier, E. (2012). A Programmable Dual-RNA–Guided DNA Endonuclease in Adaptive Bacterial Immunity. *Science*, *337*(6096), 816–821. https://doi.org/10.1126/science.1225829

Johnson, S. B., Blum, R. W., & Giedd, J. N. (2009). Adolescent Maturity and the Brain: The Promise and Pitfalls of Neuroscience Research in Adolescent Health Policy. *Journal of Adolescent Health*, *45*(3), 216–221. https://doi.org/10.1016/j.jadohealth.2009.05.016

Juarez, P., & Martínez Cerdeño, V. (2022). Parvalbumin and parvalbumin chandelier interneurons in autism and other psychiatric disorders. *Frontiers in Psychiatry*, *13*, 913550. https://doi.org/10.3389/fpsyt.2022.913550

Kitagawa, H., Tsutsumi, K., Tone, Y., & Sugahara, K. (1997). Developmental Regulation of the Sulfation Profile of Chondroitin Sulfate Chains in the Chicken Embryo Brain. *Journal of Biological Chemistry*, *272*(50), 31377–31381. https://doi.org/10.1074/jbc.272.50.31377

Kroes, A. C. M. (2010). Parvoviruses. In *Infectious Diseases* (pp. 1573–1576). Elsevier. https://doi.org/10.1016/B978-0-323-04579-7.00158-1

Kwok, J. C. F., Afshari, F., García-Alías, G., & Fawcett, J. W. (2008). Proteoglycans in the central nervous system: Plasticity, regeneration and their stimulation with chondroitinase ABC. *Restorative Neurology and Neuroscience*, *26*(2–3), 131–145.

Kwok, J. C. F., Carulli, D., & Fawcett, J. W. (2010). In vitro modeling of perineuronal nets: Hyaluronan synthase and link protein are necessary for their formation and integrity: Hyaluronan synthase and link protein in PNNs. *Journal of Neurochemistry*, no-no. https://doi.org/10.1111/j.1471-4159.2010.06878.x

Kwok, J. C. F., Dick, G., Wang, D., & Fawcett, J. W. (2011). Extracellular matrix and perineuronal nets in CNS repair. *Developmental Neurobiology*, *71*(11), 1073–1089. https://doi.org/10.1002/dneu.20974

Lam, D., Enright, H. A., Cadena, J., Peters, S. K. G., Sales, A. P., Osburn, J. J., Soscia, D. A., Kulp, K. S., Wheeler, E. K., & Fischer, N. O. (2019). Tissue-specific extracellular matrix accelerates the formation of neural networks and communities in a neuron-glia co-culture on a multi-electrode array. *Scientific Reports*, *9*(1), 4159. https://doi.org/10.1038/s41598-019-40128-1

Laubach, M., Amarante, L. M., Swanson, K., & White, S. R. (2018). What, If Anything, Is Rodent Prefrontal Cortex? *Eneuro*, *5*(5), ENEURO.0315-18.2018. https://doi.org/10.1523/ENEURO.0315-18.2018

Le Rhun, A., Escalera-Maurer, A., Bratovič, M., & Charpentier, E. (2019). CRISPR-Cas in *Streptococcus pyogenes*. *RNA Biology*, *16*(4), 380–389. https://doi.org/10.1080/15476286.2019.1582974

Lensjø, K. K., Christensen, A. C., Tennøe, S., Fyhn, M., & Hafting, T. (2017). Differential Expression and Cell-Type Specificity of Perineuronal Nets in Hippocampus, Medial Entorhinal Cortex, and Visual Cortex Examined in the Rat and Mouse. *Eneuro*, *4*(3), ENEURO.0379-16.2017. https://doi.org/10.1523/ENEURO.0379-16.2017

Lensjø, K. K., Lepperød, M. E., Dick, G., Hafting, T., & Fyhn, M. (2017). Removal of Perineuronal Nets Unlocks Juvenile Plasticity Through Network Mechanisms of Decreased Inhibition and Increased Gamma Activity. *The Journal of Neuroscience*, *37*(5), 1269–1283. https://doi.org/10.1523/JNEUROSCI.2504-16.2016

Levelt, C. N., & Hübener, M. (2012). Critical-Period Plasticity in the Visual Cortex. *Annual Review of Neuroscience*, *35*(1), 309–330. https://doi.org/10.1146/annurev-neuro-061010-113813

Levy, C., Brooks, J. M., Chen, J., Su, J., & Fox, M. A. (2015). Cell-specific and developmental expression of lectican-cleaving proteases in mouse hippocampus and neocortex: Lectican-Cleaving Proteases. *Journal of Comparative Neurology*, *523*(4), 629–648. https://doi.org/10.1002/cne.23701

Li, C., & Samulski, R. J. (2020). Engineering adeno-associated virus vectors for gene therapy. *Nature Reviews Genetics*, *21*(4), 255–272. https://doi.org/10.1038/s41576-019-0205-4

Lin, R., Kwok, J. C. F., Crespo, D., & Fawcett, J. W. (2007). Chondroitinase ABC has a long-lasting effect on chondroitin sulphate glycosaminoglycan content in the injured rat brain. *Journal of Neurochemistry*, *0*(0), 071116233414006-??? https://doi.org/10.1111/j.1471-4159.2007.05066.x

Lupori, L., Totaro, V., Cornuti, S., Ciampi, L., Carrara, F., Grilli, E., Viglione, A., Tozzi, F., Putignano, E., Mazziotti, R., Amato, G., Gennaro, C., Tognini, P., & Pizzorusso, T. (2023). *A Comprehensive Atlas of Perineuronal Net Distribution and Colocalization with Parvalbumin in the Adult Mouse Brain* [Preprint]. Neuroscience. https://doi.org/10.1101/2023.01.24.525313

Maeda, N., He, J., Yajima, Y., Mikami, T., Sugahara, K., & Yabe, T. (2003). Heterogeneity of the Chondroitin Sulfate Portion of Phosphacan/6B4 Proteoglycan Regulates Its Binding Affinity for Pleiotrophin/Heparin Binding Growth-associated Molecule. *Journal of Biological Chemistry*, *278*(37), 35805–35811. https://doi.org/10.1074/jbc.M305530200

Matthews, R. T., Kelly, G. M., Zerillo, C. A., Gray, G., Tiemeyer, M., & Hockfield, S. (2002). Aggrecan Glycoforms Contribute to the Molecular Heterogeneity of Perineuronal Nets. *The Journal of Neuroscience*, *22*(17), 7536–7547. https://doi.org/10.1523/JNEUROSCI.22-17-07536.2002

Meier, A. F., Fraefel, C., & Seyffert, M. (2020). The Interplay between Adeno-Associated Virus and Its Helper Viruses. *Viruses*, *12*(6), 662. https://doi.org/10.3390/v12060662

Mencio, C. P., Hussein, R. K., Yu, P., & Geller, H. M. (2021). The Role of Chondroitin Sulfate Proteoglycans in Nervous System Development. *Journal of Histochemistry & Cytochemistry*, *69*(1), 61–80. https://doi.org/10.1369/0022155420959147

Miao, Q.-L., Ye, Q., & Zhang, X.-H. (2014). Perineuronal net, CSPG receptor and their regulation of neural plasticity. *Sheng Li Xue Bao: [Acta Physiologica Sinica]*, *66*(4), 387–397.

Miller, E. K., & Cohen, J. D. (2001). An Integrative Theory of Prefrontal Cortex Function. *Annual Review of Neuroscience*, *24*(1), 167–202. https://doi.org/10.1146/annurev.neuro.24.1.167

Miyata, S., & Kitagawa, H. (2016). Chondroitin 6-Sulfation Regulates Perineuronal Net Formation by Controlling the Stability of Aggrecan. *Neural Plasticity*, *2016*, 1–13. https://doi.org/10.1155/2016/1305801

Miyata, S., Komatsu, Y., Yoshimura, Y., Taya, C., & Kitagawa, H. (2012). Persistent cortical plasticity by upregulation of chondroitin 6-sulfation. *Nature Neuroscience*, *15*(3), 414–422. https://doi.org/10.1038/nn.3023

Moon, L. D. F., Asher, R. A., Rhodes, K. E., & Fawcett, J. W. (2001). Regeneration of CNS axons back to their target following treatment of adult rat brain with chondroitinase ABC. *Nature Neuroscience*, *4*(5), 465–466. https://doi.org/10.1038/87415

Nahar, L., Delacroix, B. M., & Nam, H. W. (2021). The Role of Parvalbumin Interneurons in Neurotransmitter Balance and Neurological Disease. *Frontiers in Psychiatry*, *12*, 679960. https://doi.org/10.3389/fpsyt.2021.679960

Oh, Y.-M., Karube, F., Takahashi, S., Kobayashi, K., Takada, M., Uchigashima, M., Watanabe, M., Nishizawa, K., Kobayashi, K., & Fujiyama, F. (2017). Using a novel PV-Cre rat model to characterize pallidonigral cells and their terminations. *Brain Structure and Function*, *222*(5), 2359–2378. https://doi.org/10.1007/s00429-016-1346-2

Pavlov, I. P. (1906). The Huxley Lecture ON THE SCIENTIFIC INVESTIGATION OF THE PSYCHICAL FACULTIES OR PROCESSES IN THE HIGHER ANIMALS. *The Lancet*, *168*(4336), 911–915. https://doi.org/10.1016/S0140-6736(00)67165-9

Piiponniemi, T. O., Bragge, T., Vauhkonen, E. E., Vartiainen, P., Puoliväli, J. T., Sweeney, P. J., & Kopanitsa, M. V. (2017). Acquisition and reversal of visual discrimination learning in APPSwDI/Nos2−/− (CVN) mice. *Neuroscience Letters*, *650*, 126–133. https://doi.org/10.1016/j.neulet.2017.04.049

Pizzorusso, T., Medini, P., Berardi, N., Chierzi, S., Fawcett, J. W., & Maffei, L. (2002). Reactivation of Ocular Dominance Plasticity in the Adult Visual Cortex. *Science*, *298*(5596), 1248–1251. https://doi.org/10.1126/science.1072699

Pourcel, C., Touchon, M., Villeriot, N., Vernadet, J.-P., Couvin, D., Toffano-Nioche, C., & Vergnaud, G. (2019). CRISPRCasdb a successor of CRISPRdb containing CRISPR arrays and cas genes from complete genome sequences, and tools to download and query lists of repeats and spacers. *Nucleic Acids Research*, gkz915. https://doi.org/10.1093/nar/gkz915

Qi, L. S., Larson, M. H., Gilbert, L. A., Doudna, J. A., Weissman, J. S., Arkin, A. P., & Lim, W. A. (2013). Repurposing CRISPR as an RNA-Guided Platform for Sequence-Specific Control of Gene Expression. *Cell*, *152*(5), 1173–1183. https://doi.org/10.1016/j.cell.2013.02.022

Rittenhouse, E., Dunn, L. C., Cookingham, J., Calo, C., Spiegelman, M., Dooher, G. B., & Bennett, D. (1978). Cartilage matrix deficiency (*cmd*): A new autosomal recessive lethal mutation in the mouse. *Development*, *43*(1), 71–84. https://doi.org/10.1242/dev.43.1.71

Robbins, T. W., & Arnsten, A. F. T. (2009). The Neuropsychopharmacology of Fronto-Executive Function: Monoaminergic Modulation. *Annual Review of Neuroscience*, *32*(1), 267–287. https://doi.org/10.1146/annurev.neuro.051508.135535

Romberg, C., Yang, S., Melani, R., Andrews, M. R., Horner, A. E., Spillantini, M. G., Bussey, T. J., Fawcett, J. W., Pizzorusso, T., & Saksida, L. M. (2013). Depletion of perineuronal nets enhances recognition memory and long-term depression in the perirhinal cortex. *The Journal of Neuroscience: The Official Journal of the Society for Neuroscience*, *33*(16), 7057–7065. https://doi.org/10.1523/JNEUROSCI.6267-11.2013

Rossier, J., Bernard, A., Cabungcal, J.-H., Perrenoud, Q., Savoye, A., Gallopin, T., Hawrylycz, M., Cuénod, M., Do, K., Urban, A., & Lein, E. S. (2015). Cortical fast-spiking parvalbumin interneurons enwrapped in the perineuronal net express the metallopeptidases Adamts8, Adamts15 and Neprilysin. *Molecular Psychiatry*, *20*(2), 154–161. https://doi.org/10.1038/mp.2014.162

Rowlands, D., Lensjø, K. K., Dinh, T., Yang, S., Andrews, M. R., Hafting, T., Fyhn, M., Fawcett, J. W., & Dick, G. (2018). Aggrecan Directs Extracellular Matrix-Mediated Neuronal Plasticity. *The Journal of Neuroscience*, *38*(47), 10102–10113. https://doi.org/10.1523/JNEUROSCI.1122-18.2018

Russell, W. M. S., & Burch, R. L. (1959). *The Principles of Humane Experimental Technique*. Methuen. http://117.239.25.194:7000/jspui/bitstream/123456789/1342/1/PRILIMINERY%20%20AND%20%20CONTENTS.pdf

Slaker, M., Churchill, L., Todd, R. P., Blacktop, J. M., Zuloaga, D. G., Raber, J., Darling, R. A., Brown, T. E., & Sorg, B. A. (2015). Removal of Perineuronal Nets in the Medial Prefrontal Cortex Impairs the Acquisition and Reconsolidation of a Cocaine-Induced Conditioned Place Preference Memory. *The Journal of Neuroscience*, *35*(10), 4190–4202. https://doi.org/10.1523/JNEUROSCI.3592-14.2015

Song, I., & Dityatev, A. (2018). Crosstalk between glia, extracellular matrix and neurons. *Brain Research Bulletin*, *136*, 101–108. https://doi.org/10.1016/j.brainresbull.2017.03.003

Spring, S., Lerch, J. P., & Henkelman, R. M. (2007). Sexual dimorphism revealed in the structure of the mouse brain using three-dimensional magnetic resonance imaging. *NeuroImage*, *35*(4), 1424–1433. https://doi.org/10.1016/j.neuroimage.2007.02.023

Tanenbaum, M. E., Gilbert, L. A., Qi, L. S., Weissman, J. S., & Vale, R. D. (2014). A protein-tagging system for signal amplification in gene expression and fluorescence imaging. *Cell*, *159*(3), 635–646. https://doi.org/10.1016/j.cell.2014.09.039

Theocharis, A. D., Skandalis, S. S., Gialeli, C., & Karamanos, N. K. (2016). Extracellular matrix structure. *Advanced Drug Delivery Reviews*, *97*, 4–27. https://doi.org/10.1016/j.addr.2015.11.001

Thompson, E. H., Lensjø, K. K., Wigestrand, M. B., Malthe-Sørenssen, A., Hafting, T., & Fyhn, M. (2018). Removal of perineuronal nets disrupts recall of a remote fear memory. *Proceedings of the National Academy of Sciences*, *115*(3), 607–612. https://doi.org/10.1073/pnas.1713530115

Thorndike, E. L. (1905). *The elements of psychology.* A G Seiler. https://doi.org/10.1037/10881-000

Tsien, R. Y. (2013). Very long-term memories may be stored in the pattern of holes in the perineuronal net. *Proceedings of the National Academy of Sciences*, *110*(30), 12456–12461. https://doi.org/10.1073/pnas.1310158110

Tsilibary, E., Tzinia, A., Radenovic, L., Stamenkovic, V., Lebitko, T., Mucha, M., Pawlak, R., Frischknecht, R., & Kaczmarek, L. (2014). Neural ECM proteases in learning and synaptic plasticity. In *Progress in Brain Research* (Vol. 214, pp. 135–157). Elsevier. https://doi.org/10.1016/B978-0-444-63486-3.00006-2

Turner, K. M., Simpson, C. G., & Burne, T. H. J. (2017). Touchscreen-based Visual Discrimination and Reversal Tasks for Mice to Test Cognitive Flexibility. *Bio-Protocol*, *7*(20), e2583. https://doi.org/10.21769/BioProtoc.2583

Van Den Broeck, L., Hansquine, P., Callaerts-Vegh, Z., & D'Hooge, R. (2019). Impaired Reversal Learning in APPPS1-21 Mice in the Touchscreen Visual Discrimination Task. *Frontiers in Behavioral Neuroscience*, *13*, 92. https://doi.org/10.3389/fnbeh.2019.00092

Wang, D., & Fawcett, J. (2012). The perineuronal net and the control of CNS plasticity. *Cell and Tissue Research*, *349*(1), 147–160. https://doi.org/10.1007/s00441-012-1375-y

Wang, D., Tai, P. W. L., & Gao, G. (2019). Adeno-associated virus vector as a platform for gene therapy delivery. *Nature Reviews Drug Discovery*, *18*(5), 358–378. https://doi.org/10.1038/s41573-019-0012-9

Wang, X., Xu, Z., Tian, Z., Zhang, X., Xu, D., Li, Q., Zhang, J., & Wang, T. (2017). The EF-1α promoter maintains high-level transgene expression from episomal vectors in transfected CHO-K1 cells. *Journal of Cellular and Molecular Medicine*, *21*(11), 3044–3054. https://doi.org/10.1111/jcmm.13216

Yang, S., Gigout, S., Molinaro, A., Naito-Matsui, Y., Hilton, S., Foscarin, S., Nieuwenhuis, B., Tan, C. L., Verhaagen, J., Pizzorusso, T., Saksida, L. M., Bussey, T. M., Kitagawa, H., Kwok, J. C. F., & Fawcett, J. W. (2021). Chondroitin 6-sulphate is required for neuroplasticity and memory in ageing. *Molecular Psychiatry*, *26*(10), 5658–5668. https://doi.org/10.1038/s41380-021-01208-9

Yates, S. C., Groeneboom, N. E., Coello, C., Lichtenthaler, S. F., Kuhn, P.-H., Demuth, H.-U., Hartlage-Rübsamen, M., Roßner, S., Leergaard, T., Kreshuk, A., Puchades, M. A., & Bjaalie, J. G. (2019). QUINT: Workflow for Quantification and Spatial Analysis of Features in Histological Images From Rodent Brain. *Frontiers in Neuroinformatics*, *13*, 75. https://doi.org/10.3389/fninf.2019.00075

Zhang, S., Xu, M., Chang, W.-C., Ma, C., Hoang Do, J. P., Jeong, D., Lei, T., Fan, J. L., & Dan, Y. (2016). Organization of long-range inputs and outputs of frontal cortex for top-down control. *Nature Neuroscience*, *19*(12), 1733–1742. https://doi.org/10.1038/nn.4417

Appendix A – Animal information

Supplementary table 1: Animals used in the experiment.

Coordinates:

$MPFC_1$: AP +1.8, ML ±0.5, DV -2.0 & -2.5

$MPFC_2$: AP +2.0, ML ±0.4, DV -1.8 & -2.0

Viral constructs:

1. pAAV-EF1a-C6ST-1-mScarlet
2. pAAV-SCP1-dSa VPR mini. -2X snRP-1 BsaI gRNA
3. pAAV-CAG-mNeonGreen
4. pAAV-FLEX tdTomato

Experimental group								
Animal ID	Strain	Sex	Age (w)	Injection site	Viral construct(s)	Data inclusion		Surgeon
						Behaviour	Imaging	
168	C57BL/6	F	12	$MPFC_1$	1, 2	+	+	Sandra
170	C57BL/6	F	12	$MPFC_1$	1, 2	+	+	Sandra
172	C57BL/6	F	12	$MPFC_1$	1, 2	+	+	Sandra
174	C57BL/6	F	12	$MPFC_1$	1, 2	+	+	Sandra
178	C57BL/6	F	12	$MPFC_1$	1, 2	+	+	Sandra
181	C57BL/6	F	12	$MPFC_1$	1, 2	+	+	Sandra
202	C57BL/6	F	12	$MPFC_2$	1, 2	+	+	Sandra
206	C57BL/6	F	12	$MPFC_2$	1, 2	+	+	Sandra
207	C57BL/6	F	12	$MPFC_2$	1, 2	+	+	Sandra
Control group								
166	C57BL/6	F	12	$MPFC_1$	3	+	+	Sandra
169	C57BL/6	F	12	$MPFC_1$	3	+	+	Sandra
171	C57BL/6	F	12	$MPFC_1$	3	+	+	Sandra
173	C57BL/6	F	12	$MPFC_1$	3	+	+	Sandra

175	C57BL/6	F	12	$MPFC_1$	3	+	+	Sandra
178	C57BL/6	F	12	$MPFC_1$	3	+	+	Sandra
201	C57BL/6	F	12	$MPFC_2$	3	-	+	Sandra
203	C57BL/6	F	12	$MPFC_2$	3	+	+	Sandra
Viral vector testing								
301	C57BL/6	M	16	$MPFC_2$	2, 4	-	+	Sandra
302	C57BL/6	M	16	$MPFC_2$	1	-	+	Sandra

Supplementary table 2: Injection success and viral spread.

Mouse ID	Prelimbic (PL)	Infralimbic (IL)	Injection	Shared areas of viral injections
168	Both hemispheres	Both hemispheres	Bilateral	• Olfactory area • Anterior olfactory nucleus • Nucleus accumbens • Dorsal penduncular area • Orbital area • Taenia tecta • Lateral septal nucleus • Caudoputamen • Anterior cingulate area • Septho hippocampal area • Striatum
202	Both hemispheres	Both hemispheres	Bilateral	• Secondary motor area • Anterior cingulate area • Orbital area • Olfactory area • Anterior olfactory nucleus • Taenia tecta • Dorsal peduncular area • Corpus callosum • Nucleus accumbens • Striatum • Caudoputamen • Lateral septal nucleus • Septohippocampal area • Indusesum griseum
206	Both hemispheres	Both hemispheres	Bilateral	• Secondary motor area • Anterior cingulate area • Orbital area • Olfactory area • Taenia tecta • Dorsal peduncular area • Caudoputamen • Induseum griseum • Striatum • Lateral septal nucleus
207	Both hemispheres	Both hemispheres	Bilateral	• Secondary motor area • Nucleus accumbens • Olfactory areas • Dorsal peduncular area • Anterior cingulate area • Orbital area • Taenia tecta • Striatum • Anterior olfactory nucleus • Caudoputamen
170	Both hemispheres	One hemisphere	Mix	• Olfactory area • Anterior olfactory nucleus • Nucleus accumbens • Taenia tecta • Dorsal penduncular area • Secondary motor area • Caudoputamen • Anterior cingulate area

172	Both hemispheres	One hemisphere	Mix	• Dorsal penduncular area • Olfactory area • Nucleus accumbens • Anterior olfactory nucleus • Anterior cingulate area • Taenia tecta • Caudoputamen • Striatum • Dorsal penduncular area
181	Both hemispheres	One hemisphere	Mix	• Olfactory area • Anterior olfactory nucleus • Nucleus accumbens • Dorsal peduncular area • Taenia tecta • Anterior cingulate area • Secondary motor area • Caudoputamen
174	One hemisphere	One hemisphere	Unilateral	• Olfactory area • Anterior olfactory nucleus • Nucleus accumbens • Taenia tecta • Dorsal penduncular area • Caudoputamen • Anterior cingulate area • Striatum • Lateral septal nucleus • Taenia tecta
179	One hemisphere	One hemisphere	Unilateral	• Dorsal penduncular area • Taenia tecta • Anterior olfactory nucleus • Anterior cingulate area • Striatum

Appendix B – Antibodies and staining

Supplementary table 3: List of primary- and secondary- antibodies and stains

Antibody	Reactivity	Host species	Dilution	Catalog no.	Supplier
Primary antibodies					
Lectin from Wisteria floribunda-biotin conjugated	WFA	N/A	1:200	L1516	Sigma Aldrich, Germany
Anti-Aggrecan	Aggrecan	Rabbit	1:200	AB1031	Milipore Mereck, Germany
Anti-ADAMTS15	ADAMTS15	Rabbit	1:20	NBP1-86209	Novus Biologicals, USA
Anti-ADAMTS15	ADAMTS15	Rabbit	1:20	AD1126-SP	Novus Biologicals, USA
Versican	Versican	Rabbit	1:200	PB9453	Boster Biological, USA
Tenascin-R	Tenascin-R	Mouse	1:200	MAB1624	R&D, USA
GenCRISPR™ SaCas9	SaCas9	Mouse	1:200	A01951-40	Genscript, New Jersey, USA
Secondary antibodies					
Streptavidin ®CF 633 conjugate	Streptavidin	Biotin	1:200	79037	Biotium, San Francisco Bay, USA
CF568 IgG	Chicken	Rabbit	1:1000	20339	Biotium, San Francisco Bay, USA
Alexa Fluor™ 488	Goat	Chicken	1:1000	A11039	Invitrogen, ThermoFisher Scientific
Stain					
NeuroTrace™ 435/455 Blue Fluorescent Nissl stain	Nissl bodies	N/A	1:100	N21479	Invitrogen, ThermoFisher, Norway

Appendix C – Supplementary Figures

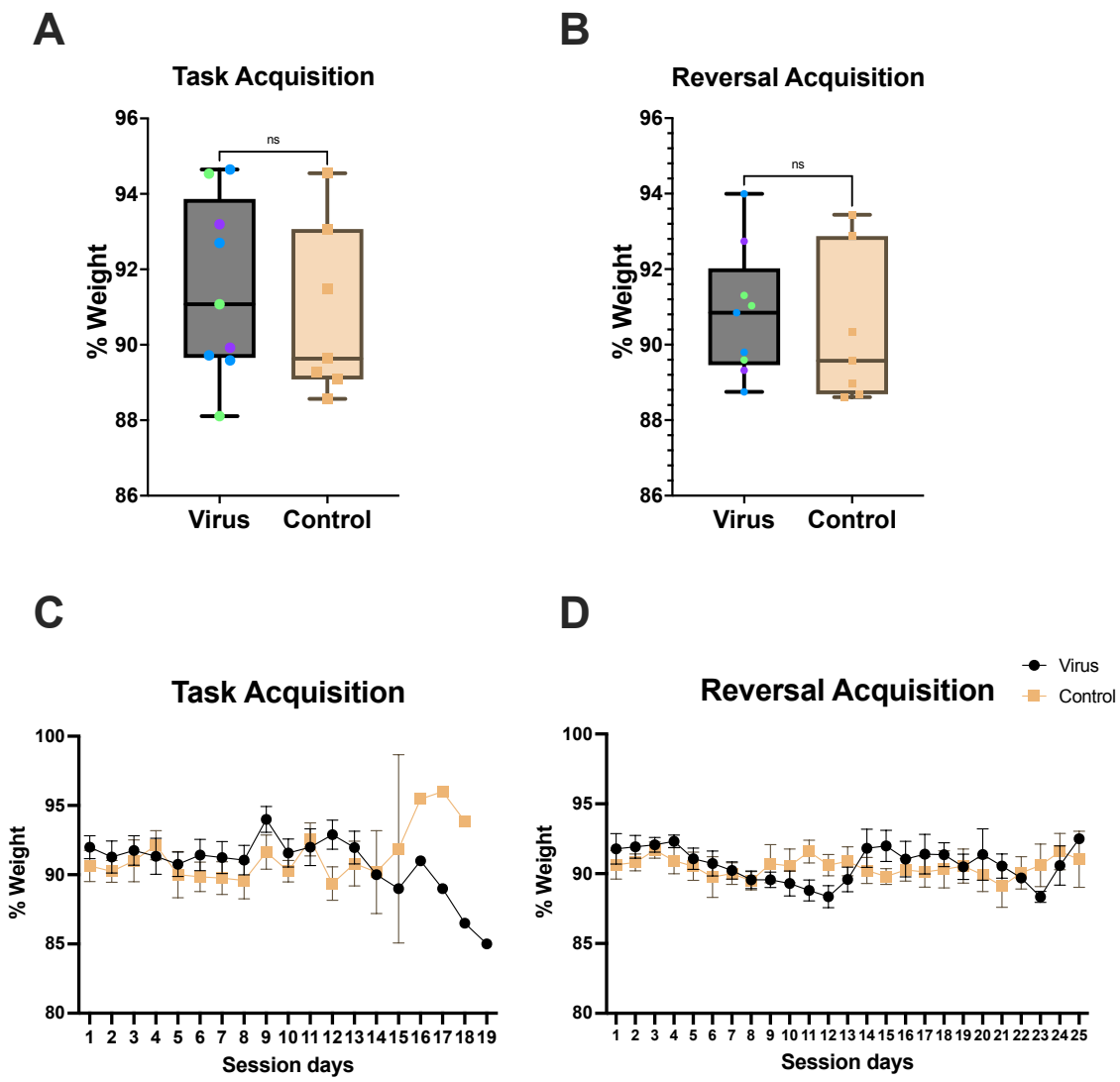

Supplementary Figure 1: Percent weight of experimental and control animals. Each dot represents the average percent weight for each mouse for the experiment. Blue dots indicate a bilateral injection of PL and IL, green dots for unilateral + IL on the other hemisphere (mix), and purple for unilateral. XY plots are presented as mean ± SEM. Boxplots display the minimum and maximum values, first and third quartile and the median**. A)** Percent weight for experimental and control group for task acquisition, measured by unpaired parametric t-test, p-value = 0.7616. **B)** Percent weight for experimental and control group for reversal acquisition, measured by Mann Whitney U test, p-value = 0.5360. **C)** Weight progression over the course of days for both groups for task acquisition. **D)** Weight progression over the course of days for both groups for reversal acquisition.

Appendix D – Immunostaining protocol

The MAXpack™ Immunostaining Media Kit (Active Motif, Belgium) was used for immunostaining.

Solutions:

- MAXpack™ Immunostaining Media Kit:
  - MAXwash washing medium
  - MAXblock blocking medium
  - MAXbind staining medium
- Phosphate buffered saline (PBS)
- Milli-Q water
- Ethanol 70%
- FluorSave mounting media
- Xylene
- Entellan

1) Wash sections 3 x 5 minutes in MAXwash washing medium
2) Incubate in MAXblock blocking medium for 1 hour at room temperature
3) Incubate in primary antibody solution (primary antibodies + MAXbind staining medium) overnight or for 3 days at 4°C.
    a) Cover plate with parafilm to prevent evaporation of the solution
4) Wash 3 x 5 minutes in MAXwash washing medium
5) Incubate in secondary antibody solution (secondary antibodies + MAXbind staining medium) overnight or for 1 day at 4°C.
    a) NeuroTrace fluorescent Nissl stain can be added to the secondary solution
6) Wash 3 x 5 minutes in MAXwash washing medium
7) Incubate in 10 minutes with wash medium or PBS with DAPI (skip this step if using Nissl)
8) Wash 2 x 5 minutes in MAXwash washing medium
9) Mount sections on glass slides and allow to dry completely
10) Rinse slide in MQ water once dry to remove any excess salts and wait until completely dry
11) Coverslip:
    a) FluorSave:
        i. Add a drop of FluorSave solution on the slices and place a cover glass on top, making sure there are no bubbles.
        ii. Leave to dry completely in a dark place.
        iii. Clean slides with ethanol and lens paper to remove any residues.
    b) Xylene-Entellan: all steps in this protocol needs to be performed in a fume hood
        i. Place the slides in xylene for 5 minutes to remove fat from the slices
        ii. Add entellan on top of the slices and place a cover glass on top while squeezing the bubbles out.
        iii. Leave to dry completely (over night or longer) in a dark place/box
        iv. Use a scalpel to remove the excess entellan once dry
        v. Clean slides with ethanol and lens paper to remove any residues.

Notes: All incubation and wash steps take place on a platform shaker, ~150 rpm.